Chapter 1

Energetic Ground State Calculations, Electronic Band Structure at Surfaces

1.1 Introduction

Energetic ground state calculation and Electronic band structure at surfaces are an important field of research in surface science, since crystallographic surfaces have been grown under ultra high vacuum conditions and several surface sensitive techniques have been developed. Currently clean, almost 2D periodic surfaces can be obtained even after adsorbing complex organic molecules.

Adsorption is a very relevant phenomenon and well known are its implications to corrosion, heterogeneous catalysis and more recently to organic electronics. But the understanding of such processes requires that of bonding of atoms and molecules at solid surfaces. Nowadays a joint experimental and theoretical efforts, based on first principles calculations, strongly propelled by the enormously increased computer power, is often successful in determining adsorption sites, geometry, possible surface reconstruction, orientation of molecules, potential energy barriers, wavefunctions, vibrations, and more recently in a few cases many-body properties such as plasmon, polariton on metals, magnons, etc.. The density of states of the clean surface and of that of the projected surface bands onto the molecular eigenstates enjoy now clearer pictures. We can distinguish surface projected bulk states, resonant surface ones but also localized surface electronic states. Refined two photon photoemission experiments or inverse photoemission ones have detected image potential states determined by the long range Coulomb tails of the surface potential. Quantum well states localized between an adsorbate overlayer and the surface are also important. Surface states can be used as a tool to monitor adsorption but may also occur as a consequence of such phenomena.

The study of molecule-surface interaction boast a great variety of systems and of

physical and chemical properties. Large binding energy implies chemisorption. This is often the case of open shell atoms, while inorganic molecules may form strong bonds or dissociate by unsaturated states on the surface. In this respect alkali adatoms are bench mark systems of which the knowledge is not only remarkable but reveal unexpected phenomena such the "vertical diffusion" probed by ^{3}He scattering. Physisorption is relevant in the simpler noble gas-solid interaction but often also dictates the coupling both in an overlayer or in a thin film of organic molecules. Adsorption of organic molecules has opened up new research perspectives. In fact such moieties display an almost infinite possibility of combining atoms to the required functionalization. Studies have in particular focused on hybrid interfaces in which an organic overlayer is adsorbed on an inorganic one, in view of applications to photovoltaics and electronic devices. Here molecular π and σ states may couple to the substrate and the van der Waals interaction often plays a crucial role.

1.2 Density Functional Theory at surfaces

Reliable theoretical models of the electronic properties of surfaces are paramount to interpret measurements, to account for the molecule surface interaction and to suggest new routes to the experimental activity. In this respect density functional theory (DFT) is currently the most popular method because first it is an ab initio approach and second, on the basis of Hohenberg-Kohn-Sham theorems it provides a quantum description capable to handle several hundreds atoms. Its main limitation is related to an approximate treatment of the exchange-correlation functional which is essentially semi-local in common implementations. A pairwise van der Waals interaction damped at shorter distances, is usually added to remedy such an incomplete correlation. Apart from the computational very expensive methods of theoretical chemistry, the study of ground states by DFT is sometimes implemented by many-body perturbation theory. However, the size of the system to be treated limit most of calculation to density functional theory (plus a phenomenological addition of the van der Waals coupling). Kohn-Sham eigenstates are found to provide approximate yet useful description of electronic bands even though these lie outside the realm of DFT being a ground state theory.

1.2.1 Theoretical framework

Density Functional Theory currently constitutes the only practical ab initio method for calculating the electronic properties of condensed matter systems that allow one to deal with a few thousand electrons (hundreds of atoms) [1]. Consequently it is the best approach to deal with a realistic description of adsorbate systems where the interaction between molecules and the surface require considering several layers. The DFT formalism is based on the Hohenberg-Kohn theorem which states that there is a one-to-one correspondence between the charge density $n(\mathbf{r})$ of a N interacting electron system and an external potential (up to a constant) $v_{ext}(\mathbf{r})$ [2]. In practice

a condensed matter system is fully identified by the electron-nuclei potential:

$$v_{ext}(\mathbf{r}) = -\sum_a \frac{Z_a}{|\mathbf{r} - \mathbf{R}_a|}, \tag{1.1}$$

where Z_a and $\mathbf{R}_a$ are the atomic number and coordinate, respectively, and atomic units are used throughout. The ground state charge $n(\mathbf{r})$ can be obtained by minimizing the total energy functional:

$$E[n] = \int d\mathbf{r}\ v_{ext}(\mathbf{r}) n(\mathbf{r}) + F[n] \tag{1.2}$$

with respect to variations of $n(\mathbf{r})$ over the possible ground state charge densities. The functional $F[n]$ is the Hohenberg-Kohn functional independent of the system.

However, the explicit form of $F[n]$ is not known. For this reasons Kohn and Sham resorted to constructing a viable set of single particle equations by affirming that for any electron problem one can make fictitious single particle equations, subject to an external potential $v_{eff}(\mathbf{r})$, such that the interacting system ground state density equals that of the non-interacting one $n_{eff}(\mathbf{r})$ [3]:

$$n(\mathbf{r}) = n_{eff}(\mathbf{r}). \tag{1.3}$$

The auxiliary problem equations, the so called Kohn-Sham (KS) equations, read as:

$$\left[-\frac{\nabla^2_{\mathbf{r}}}{2} + v_{eff}(\mathbf{r})\right] \varphi_i(\mathbf{r}) = \varepsilon_i \varphi_i(\mathbf{r}) \tag{1.4}$$

and

$$n(\mathbf{r}) = \sum_{i=1}^{N} |\varphi_i(\mathbf{r})|^2 \tag{1.5}$$

The KS equations can be worked out from the Hohenberg-Kohn variational principle which ensures that the functional $E[n]$ is stationary for small variations of the charge density from the one which guarantees the minimum energy, i.e., $n_{eff}(\mathbf{r})$ [3, 4]. One can find that:

$$v_{eff}(\mathbf{r}) = v_{ext}(\mathbf{r}) + v_H([n], \mathbf{r}) + v_{xc}([n], \mathbf{r}) \tag{1.6}$$

where $v_H(\mathbf{r})$ and $v_{xc}(\mathbf{r})$ are the Hartree and the exchange-correlation potential, respectively.

The KS approach is exact: its limitations regard the approximated choice of the exchange-correlation potential defined as the functional derivative of the exchange-correlation functional,

$$\frac{\delta E_{xc}[n(\mathbf{r})]}{\delta n(\mathbf{r})} = v_{xc}(\mathbf{r}). \tag{1.7}$$

Here $E_{xc}[n]$ includes the the electron-electron functional minus the Coulomb classical one plus the kinetic energy functional difference between the (unknown) correct one and the single particle expression [4]. Approximations to $E_{xc}[n]$ will be discussed in the following Section.

Finally we wish to remark some important points of the KS equations: (i) They can be solved self-consistently; (ii) they allow for a magnetic solution; (iii) differently from the Hartree-Fock approach their eigenvalues cannot be associated to ionization energies, since the Koopmans' theorem does not hold. Only the highest occupied KS eigenvalue is exactly the chemical potential of the system [5]. The KS eigenstates cannot be interpreted as one electron orbitals since the sum of the squared magnitudes of the occupied orbitals, i.e., the charge density, is the fundamental quantity in DFT. However, both eigenfunctions and eigenvalues may often be considered as one-electron orbitals and energies with a good accuracy.

The local density approximation

The local density approximation (LDA) functional can be defined by that of the exchange-correlation one for the homogeneous electron gas. Though a very simplified expression the LDA provides a useful guess for $E_{xc}[n(\mathbf{r})]$ of several condensed matter systems [3]. In a spin polarized form the LDA exchange-correlation functional can be generalized to the local spin density approximation (LSDA) to be written as:.

$$E_{xc}[n]^{LSDA}[n_\uparrow, n_\downarrow] = \int n(\mathbf{r})\varepsilon_{xc}(n_\uparrow(\mathbf{r}), n_\downarrow(\mathbf{r})d\mathbf{r} \tag{1.8}$$

where $n(\mathbf{r}) = (n_\uparrow(\mathbf{r})+n_\downarrow(\mathbf{r})$, and ε_{xc} is the exchange-correlation energy per particle for a homogeneous electron gas depending on its spin. Despite of its simple expression the L[S]DA has accomplished many relevant results [6]. For example the bulk constants, cohesive energies and bulk moduli have bee computed for C, Si, Ge with very small differences with respect to the experimental data, namely $\simeq 1\%$ for the bulk constants, $\simeq 4\%$ for the cohesive energies and $\simeq 5\%$ for the bulk moduli. A detailed LDA-DFT study has demonstrated that the diamond structure is the most stable one for Si among several plausible ones [7]. The success of L[S]DA for systems with rapid changes in $n(\mathbf{r})$ can be explained by recalling a fundamental property of the exchange-correlation hole $n_{xc}(\mathbf{r}, \mathbf{r}')$, defined as [8]:

$$n_{xc}(\mathbf{r}, \mathbf{r}') = \frac{n_2(\mathbf{r}, \mathbf{r}')}{n(\mathbf{r})} - n(\mathbf{r}), \tag{1.9}$$

where $n_2(\mathbf{r}, \mathbf{r}')$ is the diagonal second order density matrix, which represents the conditional probability of finding an electron in $\mathbf{r}'$ if there is one in $\mathbf{r}$. In an exact theory:

$$\int n_{xc}(\mathbf{r}, \mathbf{r}')d\mathbf{r}' = -1 \tag{1.10}$$

The theorem in (1.10) is satisfied by the exchange-correlation hole in L[S]DA. We also observe that while the function $n_{xc}(\mathbf{r}, \mathbf{r}')$ is poorly estimated by L[S]DA, the corresponding exchange-correlation functional E_{xc}^{LSDA}:

$$\begin{aligned} E_{xc}^{LSDA} &= \frac{1}{2}\int d\mathbf{r}\ n(\mathbf{r}) \int d\mathbf{r}' \frac{1}{|\mathbf{r}-\mathbf{r}'|} n_{xc}(\mathbf{r}, \mathbf{r}') \\ &= \frac{1}{2}\int d\mathbf{r} \int_0^\infty R^2 dR \frac{1}{R} \int d\Omega\ n_{xc}(\mathbf{r}, \mathbf{R}) \end{aligned} \tag{1.11}$$

only depends on the spherical average of $n_{xc}(\mathbf{r}, \mathbf{R})$ so that E_{xc}^{LSDA} is often a reliable approximation to the exchange correlation energy, since such a functional displays only a weak dependence on the exact shape of the exchange correlation hole [9].

The Generalized Gradient Approximation

Though being a very useful approximation, the L[S]DA is often unable to supply quantitative correct predictions of physical quantities, e.g., it overestimates dissociation energies by about 1 eV and finds out inaccurate molecular atomization energies which turn out to be about 1 eV smaller than the real ones [10]. All these errors are much above the chemical accuracy of 43.36 meV. To amend such discrepancies it looked rather obvious to introduce a semilocal exchange-correlation functional also dependent on the charge density. This expression is named the the Generalized Gradient Approximation (GGA) in which the exchange correlation functional E_{xc}^{GGA} is given by:

$$E_{xc}^{GGA} = \int f\big(n_{\uparrow}(\mathbf{r}), n_{\downarrow}((\mathbf{r}), \nabla n_{\uparrow}(\mathbf{r}), \nabla n_{\downarrow}(\mathbf{r})\big) d\mathbf{r} \tag{1.12}$$

Note that (1.12) is called generalized gradient approximation because E_{xc}^{GGA} does not simply include a gradient expansion of the exchange-correlation functional as it occurs in the gradient expansion approximation. Such approach does not fulfill some fundamental properties of the exchange-correlation hole and hence causes results worse than those by L[S]DA. The merit of the GGA is to describe the exchange correlation hole more realistically than a sheer expansion in the density. To this aim real space cutoffs are introduced, and in analogy to L[S]DA the exchange hole is never positive, while the exchange and correlation holes integrate to minus one and zero, respectively [9, 11, 12, 13].

In [14] the GGA is extensively applied to several systems with consistent improvements in the calculated properties. First ionization energies of thirty atoms and atomization ones of simple hydrocarbons agree with the experimental ones within a 10 % error. For three metals (Al, Na, Cs) studied with the stabilized jellium model very good estimates of the work function and the surface energy have been worked out [15]. The GGA functional unlike the L[S]DA is not unique and may contain empirical parameters. Among the most successful ones we recall the functional by Perdew and Wang (PW91) [11, 12, 13, 14] by which the above mentioned results were computed; and the subsequent Perdew, Burke, and Ernzerhof (PBE) [16, 9] and the revised PBE ones [17, 18]. The PBE functional is based on the PW91 one, but it exhibits a simpler and more transparent form, only satisfies physically important conditions, provides a precise account of the linear response of the homogeneous electron gas and it scales correctly in the low and high density limit. For all these reasons the PBE functional is routinely preferred to the PW91. As a detail the revPBE functionals substitute the value of the empirical parameter κ in the exchange functional with one which best matches the exchange function of the first row atoms and allows obtaining better chemisorption energies [17, 18].

Failures of the DFT-GGA method

Despite the very good results outlined in the previous Section, the GGA functional exhibits three important drawbacks: (i) the presence of a spurious self-interaction [19]; (ii) the lack of discontinuities in the derivatives of the total energy at N integer number of particles [8, 20]; (iii) the erroneous exponential long range decay interaction of an electron with a metal surface and the inability to treat realistically the van der Waals interaction between two molecules or a molecule and a surface [21]. This last topic will be addressed later in this Section.

(i) We recall that in the Hartree-Fock method the self-interaction is correctly zero since for the same electron the Hartree and the exchange term cancel out. For an extended system of N electrons the right number of pair interactions is given by $N(N-1)/2$ and largely overcomes that of the self-interaction proportional to N. But for an atom or a small molecule the self-interaction correction (SIC) is a relevant one. For this reason a modified functional to subtract spurious terms has been suggested which corrected very well the ionization energies of atoms [19]:

$$E^{\mathrm{SIC}} = E^{approx}[n^{\uparrow}, n^{\downarrow}] - \sum_{\alpha,\sigma} \big(J[n_{\alpha,\sigma}] + E^{approx}[n_{\alpha,\sigma}, 0] \big) \tag{1.13}$$

The expression E^{approx} is a conveniently approximated classical plus exchange-correlation functional, while J is the classical Coulomb one and hence the sum represents the SIC summed over all orbitals (α, σ). In (1.13) the self-interaction is subtracted for each orbital and creates an effective potential which is orbital dependent in the KS equations. We shall come back to this problem later on.

(ii) It is well known that the variational formulation of DFT with the constraint of a fixed number of particles and external potential v_{ext} is expressed via the Lagrange multiplier μ by:

$$\delta \left(E[n] - \mu \int n(\mathbf{r}) d\mathbf{r} \right) = 0, \tag{1.14}$$

which implies

$$\delta E[n]/\delta n(\mathbf{r}) = \mu. \tag{1.15}$$

Following [22] (1.15) can be extended to non-integer number of particles N by considering a mixture of pure states with fractional occupancy as an average. By assuming that $n_N(\mathbf{r})$ is the solution of (1.14) with particle number N the corresponding energy is $E_N = E[n_N]$ and:

$$\partial E/\partial N = \mu(N). \tag{1.16}$$

So the Lagrange multiplier μ is the exact chemical potential [4, 23].

By using fractional occupancy one can get the ground state energy of the system on varying the particle number N. Such an energy is formed by piecewise segments joining with discontinuous derivatives at integer N and allows one to get the first ionization I and affinity energies A. For an atom with nuclear charge Z [4]:

$$I = E(Z-1) - E(Z), \tag{1.17}$$

$$A = E(Z) - E(Z+1). \tag{1.18}$$

This behaviour is described correctly by the exact DFT. Instead LDA and GGA calculate such fractional energies $E(Z)$ with an unphysical curvature and wrong minima at fractional occupancies. Such incorrect results are associated to the spurious self-interaction of fractional electrons introduced in the system and may be amended by adding a Hubbard-like term U to the LDA energy functional [20]: this approach is the so called LDA+U method. We finally point out that occupancies entering the LDA+U functional are expressed as projections of the KS orbitals on a suitable localized basis set. For this reason and alike SIC this functional is orbital dependent and non local.

Orbital dependent functionals

As pointed out in the previous Section, orbital dependent functionals could be a useful implementation to DFT. But we stress that in the KS equation the potential $v_{eff}(\mathbf{r})$ must be local and the same one for all orbitals to satisfy the Hohenberg-Kohn theorem [2]. So the orbitals to evaluate the exchange term must be KS orbitals which are generally different from the Hartree-Fock (HF) ones and generate an exchange energy other than the HF one and consequently two different correlation energies (i.e., the total energy, equal in all exact theories, minus the HF one) are determined in the two methods. Note that the KS orbitals depend on the charge density and are obtained solving the Schrödinger equation by a local multiplicative potential, while those computed by orbital specific potentials are not. This is an important problem [10, 24] and much work has been devoted to it outside the scope of this review. We only remind that in the optimized effective potential formalism it has been demonstrated that at first order in the density the energy functionals coincide when the variation between the KS potential and an orbital dependent one is taken into account [10, 24]. Moreover Gilber's theorem [25] established that a non local external potential determines uniquely the first order density matrix, but from a known ground state wavefunction the external potential v_{ext} is not given in a sole way [25].

A very popular class of orbital dependent functionals are the hybrid ones which incorporate part of the exact exchange term from HF. First Becke realized that the adiabatic connection formula [26, 27] could be the correct tool to obtain rigorously the exchange correlation energy E_{xc} in the KS formalism and suggested the following expression [26]:

$$E_{xc} \simeq \frac{1}{2}E_x + \frac{1}{2}E_{xc}^{LSDA} \tag{1.19}$$

where E_x is the exchange energy of the KS orbitals. Such half exchange plus half LSDA contributions was improved into a three parameter formula:

$$\begin{aligned} E_{xc}^{hyb} &= E_{xc}^{LSDA} + a_0(E_x - E_x^{LSDA}) \\ &+ a_x\Delta E_x^{GGA} + a_c\Delta E_c^{GGA} \end{aligned} \tag{1.20}$$

where ΔE_x^{GGA} and ΔE_c^{GGA} are exchange and correlation gradient corrections to their respective L[S]DA expressions [10, 27]. A popular expression for the exchange

correlation functional is that by Becke, Lee, Yang, and Parr (B3LYP) constituted by several terms with constants referred to thermochemical data. Such terms are: the LDA and HF exchange [28]; the gradient exchange correction by Becke [29]; the Lee Yang Parr correlation; the Vosko, Wilk, and Nusair to provide the coefficients of local and gradient correlation functionals [30]. With this functional one obtains excellent atomization energies for the G2 set of molecules [31], and standard enthalpies of formation, ionization, affinity energies of the G3/99 set [32]. For these reasons such a semiempirical functional is widely used especially in the chemical scientific community [10]. Several other hybrid functional have been proposed and we refer the reader to specialized papers [33, 34].

The van der Waals interaction

The van der Waals (vdW) or London dispersion interaction is a quantum effect due to the instantaneous zero-point fluctuations of electrons determining multipole moments on a quantum system which may induce other ones in other moieties, which interact with each other. Such a coupling is usually weaker than the eletrostatic one but is pervasive in materials science becoming more important for larger molecules, noble gases and organic molecule-surface systems. The polarizability of atoms, also depending on their environment, is fundamental to estimate the magnitude of the vdW forces [35, 36, 37]. The vdW coupling is attractive and behaves asymptotically as R^{-6} for two atoms/molecules at distance R, R^{-3} for a molecule surface system, R^{-2} among two metal surfaces [37]. Such an interaction is a many-body phenomenon included in the exact DFT, but is not accounted correctly by the GGA and hybrid functionals since they neglect instantaneous charge density fluctuations and correlations and solely consider semi-local correlations. The rigorous treatment of the vdW interactions should grasp their non-additive and non-local character but models with pairwise potentials and fitted parameters can achieve good qualitative results in systems stemming from hybrid interfaces to biomolecular compounds [35].

In this Chapter we would like to outline three methods capable to treat the vdW interaction within DFT and which are suited to molecule-surface systems. First the Rutgers-Chalmers collaborative efforts, say vdW DF and vdW DF2, succeeded in writing a seamless exchange-correlation functional as:

$$E_{xc}^{DF} = E_x^{GGA} + E_c^{LDA} + E_c^{nl} \tag{1.21}$$

where E_x^{GGA} is the exchange energy in the revPBE approach, E_c^{LDA} the LDA correlation energy and E_c^{nl} the non-local correlation, [38, 39, 40]. In this method one treats the non-local functional starting from the adiabatic connection formula for the exact correlation energy, [38, 40], and then makes an expansion in the integrand to second order in $\hat{\varepsilon}$, being $\hat{\varepsilon}$ the dielectric constant treated in the plasmon pole approximation. By this approach results in good agreement with experiments were calculated for the interaction energies of molecular dimers (duplexes) of the S22 complex set. A comparison with quantum chemistry results of vdW DF and vdW DF2 is shown in Fig. 1.1 [41]. The vdW DF treatment has also proven to be accurate enough to study adsorption of organic molecules on solids, see n-alkane adsorption on C(0001) deposited on Pt(111) and n-butane on Cu(100), Cu(111), Au(111) and Pt(111) [40], and to

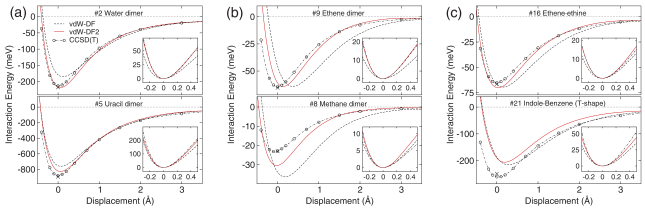

Figure 1.1: Comparison between vdW DF and quantum chemistry (CCSDT) potential energy curves, for the best and the worst case (among the S22 duplexes) of (a) hydrogen-bonded, (b) dispersion-dominated, and (c) mixed duplexes. Insets compare the shapes near the minima upon aligning to a common minimum point. Reprinted figure with permission from Kyuho Lee et al., Physical Review B, 82, 081101 (2010). Copyright (2010) by the American Physical Society. http://dx.doi.org/10.1103/PhysRevB.82.081101.

investigate adsorption of organic molecules on solids, e.g., benzene and naphthalene on graphite [42].

A semiempirical method was devised by Grimme in which the vdW dispersion interaction between a couple of atoms is assumed to have the well known asymptotic pairwise form, E_{disp}:

$$E_{disp} = s_6 \sum_{i=1}^{N_{at}-1} \sum_{j=1}^{N_{at}} \frac{C_6^{ij}}{R_{ij}^6} f_{damp}(R_{ij}) \tag{1.22}$$

and we denote the total functional as:

$$E_{DFT-D} = E_{KS-DFT} + E_{disp} \tag{1.23}$$

In (1.22) N_{at} is the number of atoms in the system, C_6^{ij} are the dispersion coefficients, R_{ij} the interatomic distances, s_6 is a scaling factor depending on the used approximate functional in the KS scheme. The damping function $f_{damp}(R_{ij})$ is equal to 1 for large R and becomes very small for R going to zero. In the D2 scheme the dispersion coefficients are given by a geometric mean of the atomic ones:

$$C_6^{ij} = \sqrt{C_6^i C_6^j}. \tag{1.24}$$

Being the coefficient C_6 proportional to the ionization potential and the static dipole polarizability, it acts as a predetermined quantity which does not take into account modications of the physical and chemical environment [43]. To consider such effect in the C_6 coefficients Grimme's group later introduced the D3 scheme which takes into account the number of neighbours of each atom [44]. The larger the coordination the smaller the coefficient C_6^i of atom i, since the atom is somewhat compressed. In the numerical procedure one starts from a reference set of C_6 coefficients for each pair of atoms depending on their properties (location, hybridization). Interpolating among them by varying the number of neighbours one can obtain continuously changing C_6

values. The accuracy of this approach is confirmed by several results discussed in [44] and makes it a very useful tool in adsorption calculations also for organic molecules [45].

A different idea to take into account the environmental effects in the calculation of C_6^{ij} is to introduce the effective volume of an atom which is different from the free one. By using a Hirshfeld atomic partitioning weight $w_A(\mathbf{r})$ for atom A, the coefficient C_6^{AA} for an atom inside a molecule or a solid is scaled by the squared ratio of its volume in the molecule/solid and in the free atom within a self-consistent procedure. Then an equation for the coefficient between two atoms C_6^{AB} is provided in terms of C_6^{AA}, C_6^{BB} and the static atomic polarizability. Finally the dispersion interaction is written as a pairwise summation alike (1.22) [46]. This is often named the Tkachenko-Scheffler PBEvdW method. Still within an atomic pair summation is the more recent one, so called vdW-surf approach [47]. In this treatment many-body effects are taken into account by employing the Lifshitz-Zaremba-Kohn theory [48] to write the dispersion coefficient which includes the polarizability of the atoms and the dielectric constant of the solid. For a realistic calculation of adsorption energies one has also to take into account rapid variation of C_6^{AB} near the surface which may be described by a varying effective dimensionless volume, V_{eff}^i, to be determined via the Hirshfeld method. The effective $C_{6,eff}^{ii}$ coefficient attains the final form $C_{6,eff}^{ii} = [V_{eff}^i]^2 C_{6,bulk}^{ii}$ [47]. Accurate estimates of geometries and adsorption energies of perylene-3,4,9,10-tetracarboxylic dianhydride (PTCDA) on noble metals and Xe and benzene on transition metal surfaces have been worked out [47, 49]. For an up to date review on vdW interaction for adsorption of organic molecules at metals, see [50].

Finally we wish to recall that both for a more accurate description of the ground state, and for excited ones, Time Dependent (TD)DFT and many-body perturbation theory are started being used with more stringent limitations of size [51].

1.2.2 Model geometries

Cluster

The cluster model was introduced for the study of catalysis describing the system, i.e., a nanoparticle or a surface with an adsorbate, by a cluster of atoms plus the admolecule. Among the advantages of such an approach the treatment of localized effects, the convenient usage of computational chemistry methods instead of those with semi-infinite substrate. Difficulties may arise for the convergence of results with the cluster size and unwanted surface effects since the cluster displays several surfaces not just the one on which the adsorbate is located. This determines a large number of uncoordinated atoms and possibly surface charges to be compensated. The cluster model has proven successful, e.g., in evaluating the optical absorption spectra of adsorbed dyes [52] and, with suitable embedding techniques, to the free energy of proton abstraction from water at $TiO_2(110)$ [53], but its relevance has historically decreased in favor of the slab one. For recent reviews on the cluster model see [54, 55].

Slab

The slab approach describes the surface plus the adsorbate as a film of few 2D periodic layers accounting for the solid plus an adsorbate overlayer usually deposited on one of the two surfaces. On the 2D periodic surface, for which the surface parallel momentum $\mathbf{K}$ is a good quantum number, by using Bloch waves as a linear combination of a set of localized orbitals l at lattice site i, say $\{\varphi_{\alpha i}\}$, the electronic energies can be obtained by the following secular equation for the wavefunction coefficient $c_{\beta j}$ [8]:

$$\sum_{\beta j}(H_{\alpha i,\beta j} - E_{\mathbf{K}} S_{\alpha i,\beta j})c_{\beta j} = 0, \tag{1.25}$$

where $H_{\alpha i,\beta j}$ are the matrix elements of the KS Hamiltonian, while $S_{\alpha i,\beta j}$ the overlap ones. A way to recover 3D periodicity in the direction $\hat{z}$ normal to the surface is to repeat the slab adding a vacuum portion between replicas which has to be wide enough to avoid the spurious interaction [56, 57, 8]. A particularly useful basis set for this 3D supercell geometry is represented by plane waves [57, 8]. If solved on a plane wave basis set, the supercell method requires a larger basis than the localized one of the 2D slab approach but matrix elements of plane waves are easier to compute and converge. Indeed, for plane wave basis sets, the only parameter is the kinetic energy cutoff that can be increased without any bias. Practically, two kinetic energy cutoffs are chosen in representing the wavefunctions ($E_{c,\psi}$) and the charge density ($E_{c,\rho}$, with $E_{c,\rho} \neq E_{c,\psi}$ to properly describe ultrasoft pseudopotentials and ones with non-local core corrections). As a matter of fact the surface study within the supercell approach translates in a bulk problem but for a 2D integration of the Brillouin zone, so the reader can be referred to textbooks on Electronic Structure calculation for practicalities [58].

The extended substrate

The models so far discussed provide computational viable methods to calculate surface properties by systems that are finite in the direction orthogonal to the surface. However, one should not ignore that the thickness of the substrate in a typical experiment is several orders of magnitude larger and hence better represented by a semi-infinite one. For this reason Green's function approaches accounting for the continuous spectrum of the solid were contrived. Such methods more recently formulated within DFT-KS include the Dyson equation [59, 60, 61], the embedded cluster [62, 63, 64] and Green's function matching techniques [65, 66, 67, 68]. Owing to the extraordinary increase of computer performances in the last two decades, capable now to handle routine DFT simulations with several hundred atoms, the above methods have become less popular than the computationally simpler supercell approach to calculate adsorption geometries and energies. Such a technique also allows to attain a very good description of bond structures, density of states (DOS) and spectroscopies of adsorbates. Only if the detailed features of narrow peaks in the adsorbate projected density of states (PDOS) are required, e.g., to get information on the elastic linewidths of surface states, the continuum of substrate states in the calculation appears to be beneficial [69]. Finally we report that recently a Green's

function approach adapted from quantum transport theory [70] has been successfully employed to the calculation of the lifetimes of the lowest unoccupied molecular orbital (LUMO) of organic molecules on rutile $TiO_2(110)$ [71] and of the LUMO of core excited pyridine on Au(111) [72], via the inverse of the linewidth of this state. The former result may help understanding charge transfer in dye sensitized solar cells, the latter one bidirectional electron transport in femtosecond phenomena. To show the computational suitability of this approach for calculating the PDOS of molecules on solids compared to the finite size models we observe that the resolution of the LUMO PDOS of perylene compounds on a $(TiO_2)_{60}$ cluster is very approximate [73]. If one assumes to adopt a slab geometry, a 2D unit cell of rutile $TiO_2(110)$ (3×1) and a required resolution of 2 meV in the PDOS for fixed surface wavevector, he is forced to use more than 50 trilayers of semiconductor which would make the calculation very cumbersome. Instead by the above Green's function method we can determine the PDOS on a molecular orbital of an adsorbate, Φ of energy E_Φ, by the imaginary part of the Green's function. Thus we can fit the result with a Lorentzian function with fwhm Γ [71]:

$$P_\Phi \propto \frac{1}{\pi} \frac{\Gamma}{(E - E_\Phi)^2 + \Gamma^2}. \tag{1.26}$$

1.3 Electronic states at surfaces

Surface intrinsic electronic states, which decay exponentially both towards vacuum and bulk, may occur when 3D bulk periodicity is broken by a surface. Traditionally they are distinguished as Shockley [74] and Tamm [75] states. The derivation of such states is extensively described in several books [76, 77], which we refer the reader to for a thorough treatment. Here it suffices to outline the main properties.

Bulk bands from the surface viewpoint

Given that bulk electronic states persist in presence of the surface, their identification in terms of the surface symmetry is a necessary prerequisite for the description of genuine surface electronic states. This calls for obtaining the so-called "surface-projected band structure". A 3D wavevector $\mathbf{k}$ is decomposed in the components parallel and perpendicular to the surface, $\mathbf{k} = \mathbf{K} + \mathbf{k}_\perp$, so that bulk Block states $\epsilon_n(\mathbf{k})$, with n the band index, can be labeled by a joint index $(n, \mathbf{k}_\perp)$ and studied as a function of $\mathbf{K}$: $\epsilon_{n,\mathbf{k}_\perp}(\mathbf{K})$. Notice that, at variance of n, $\mathbf{k}_\perp$ can span a continuum of values so that energy ranges, rather than discrete values, are allowed for $\epsilon_{n,\mathbf{k}_\perp}(\mathbf{K})$.

As an example we consider model (tight-binding) simple cubic solid, having a single band with analytic form $\epsilon(\mathbf{k}) = -V[\cos(k_x a) + \cos(k_y a) + \cos(k_z a)]$, and derive the (001) surface band structure. Namely, we are interested in the energy ranges accessible at fixed $\mathbf{K} = (k_x, k_y)$ as a function of k_z in the interval $[-\frac{\pi}{a}, \frac{\pi}{a}]$. These ranges, evaluated at the high-symmetry points of the surface Brillouin zone, are $[-3V, -V]$ for $\mathbf{K} = \bar{\Gamma}$, $[-V, V]$ for $\mathbf{K} = \bar{X}$, $[V, 3V]$ for $\mathbf{K} = \bar{M}$. Overall, the band structure depicted in Fig. 1.2 is obtained.

As a more realistic example we consider the case of a face-centered-cubic metal, Cu(111). In practical ab initio calculation a bulk conventional unit cell with three

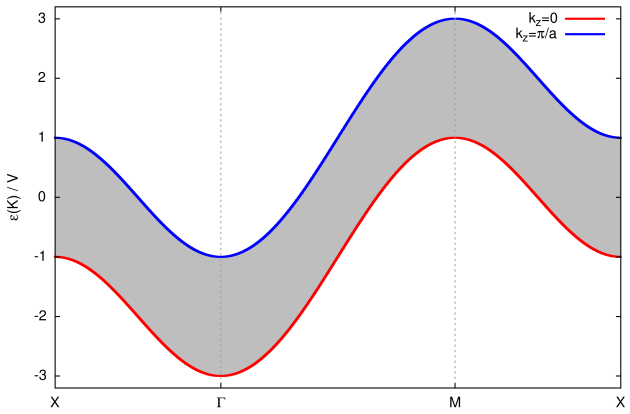

Figure 1.2: Surface band structure of a tight-binding model of a simple cubic crystal with an s-like band.

atoms following the ABC stacking of atomic planes along the (111) direction can be constructed, and the bands plotted for different values of $k_\perp$. One obtains a "spaghetti plot" becoming denser with a finer sampling of $k_\perp$, that is reported in Fig. 1.3 as a gray area. Especially interesting is the presence of bulk-forbidden energy regions (surface-projected band gaps) where surface electronic states can exist. Such plots can be compared to the electronic structure in presence of the surface. To that purpose, in Fig. 1.3 the states of a 30-atom thick Cu(111) slab are reported, corresponding to 30 possible values of $k_\perp$. There, additional features emerge, in the surface-projected band gaps or overlapping with bulk bands, that originate from the surface modification of the electronic potential and are discussed in the next paragraphs.

Shockley and Tamm states

In a simple picture of Shockley states we consider a periodic solid described by the nearly free electron model. Even if the lattice potential is treated as a small perturbation, its effect is to open up gaps in the band structure in which localized states may exist near the surface. Within the gap no solution are found for the wavevector $\mathbf{k}$ real. Formally we look for wavefunctions with complex $\mathbf{k}$ and imaginary part $k_I > 0$. Assume that the lattice periodic potential is interrupted at $z = z_0$ (z being the direction normal to the surface so that $\mathbf{r} \equiv (\mathbf{R}, z)$ by a step function of height W_0, a surface is created at $z = z_0$ and vacuum extends in the semi space $-\infty < z < z_0$. The complex wavefunction involves a factor $\exp(-k_I z)$ decreasing exponentially for positive and diverging for negative z_0, respectively. The latter solutions are incorrect for infinite bulk but are acceptable for a semi-infinite solid if they can be matched to decaying waves in vacuum of the form $\psi_{out} \propto \exp(\kappa z)\exp(i\mathbf{K}\cdot\mathbf{R})$, where κ is real and positive and equal to:

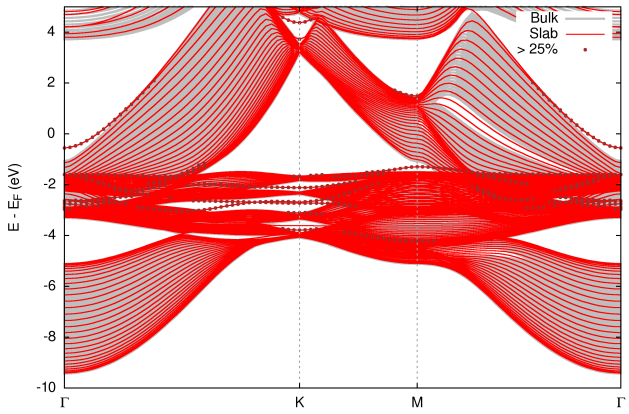

Figure 1.3: Band structure of a slab consisting of 30 Cu(111) layers, calculated at the Kohn-Sham PBE level of theory in absence of surface relaxations. Brown circles mark states whose weight on the first/last Cu layers is larger than 25%. The gray shaded area is the surface-projected band structure.

$$\kappa = \left[2\left(W_0 - E + \frac{K^2}{2}\right)\right]^{1/2} \tag{1.27}$$

By equating the logarithmic derivatives of the wavefunctions, ψ_{in}, decaying into bulk, with ψ_{out} we obtain κ. Such a state localized at the surface is named the Shockley state.

An alternative way to describe surface states is to make use of the tight-binding method which is useful when the extention of the atomic orbitals in the solid is less than the interatomic spacing and so applicable to the study of narrow bands of transition metals and actinides. In this framework consider the slab model with infinite periodic atomic planes, identical atoms and one atom per unit cell. In (1.25) one can write:

$$c_{\alpha i(p)}(\mathbf{K}) = \exp\left(i\mathbf{K}\cdot\mathbf{R}_i\right)c_{\alpha p}(\mathbf{K}) \tag{1.28}$$

where $\mathbf{R}_i$ is a 2D lattice vector while p labels the atomic plane of atom i. If P is the number of planes one solves a secular equation alike (1.25) of dimension $lP \times lP$.

An elegant approach to compute the system bands is to avail oneself of a continued fraction technique within the single particle Green's function. If we confine to a linear chain in the Hückel approximation, i.e. the resonance integral is $-\beta$ with $\beta > 0$, is non zero only for nearest neighbours while overlap is zero for orbitals in different sites, and modify the atomic orbital, say α_s for the first atom in the chain, two localized orbitals occur, that are named Tamm states. One with energy above that of the band for $\alpha_s > \beta$ and one below it for $\alpha_s < -\beta$. To take into account a simple solid with a chemisorbed atom Grimley also changed the resonance integral between the adatom and its nearest neighbour. According to the parameters one or two localized states may exist, that lying outside the band describe the formation of a localized bond [78].

A well known example of Shockley and Tamm states is provided by the noble metal surfaces. For Cu(111) angle resolve photoemission spectroscopy (ARPES) and DFT calculations [79, 80, 81] determined a fairly parabolic (sp) Shockley state, crossing the Fermi level, ε_F, along the $\bar{\Gamma}\bar{M}$ and $\bar{\Gamma}\bar{K}$ paths, with a minimum about 0.5 eV below ε_F. A d-like fairly dispersionless Tamm state was measured and computed just above the projected bulk d band around $\bar{M}$ and at about -2.0 eV below ε_F. See also Fig. 1.3. Along the direction $\bar{\Gamma}\bar{M}$ this state merges into the d band and becomes a surface resonant state, defined as a state which preserves an enhanced amplitude at the surface but propagates into bulk like a Bloch wave [82].

Quantum well states

If we deposit ultrathin layers of atoms or molecules on the surface constituted of a different material 1D potential wells could be formed in the $\hat{z}$ direction. Such systems may display localized quantized states typical of a particle in a box and hence are named quantum well (QW) states. Several examples of such states are found in semiconductor heterostructures and metal atoms on metal surfaces. For a review on the latter systems see [83].

Image States

Together with Shockley and Tamm surface states a free surface exhibit surface states generated by the image potential (IP). In classical physics if an electron is at distance z from a metal, the electron-surface interaction can be calculated by replacing it with the interaction of an electron of charge e with a positive charge $-e$ (image charge) at position z inside the metal. One obtains:

$$V_{image}^{class}(z) = -\frac{e^2}{4z}. \tag{1.29}$$

In a microscopic quantum treatment in which the metal is described by a semi-infinite jellium the distance z is substituted by that with reference to a plane with coordinate z_{image} which is the centre of gravity of the metal polarization charge [84]. At large enough distances from the surface one can write:

$$V_{image}(z) = -\frac{e^2}{4(z - z_{image})}. \tag{1.30}$$

The potential formed by the surface repulsive barrier (that occurs if a gap is present in the surface-projected bulk band structure) and $V_{image}(z)$ generates weakly bound states with wavefunctions mainly located outside the surface [85]. They constitute a Rydberg-like series with energies E_n:

$$E_n = \frac{-0.85}{(n+a)^2} \text{ eV}. \tag{1.31}$$

The constant a depends on the surface, the width of the energy gap and its position with respect to vacuum. Inverse (IPES) and two photon (2PP) photoemission spectroscopy are the experimental techniques of choice to investigate IP states (IPS).

Finally we remark a new effect for IPS due to the spin-orbit Rashba effect [86]. Measurements performed with 2PP and circular dichroism coupled to DFT calculations with the phenomenological addition of the IP and based on the Green function embedding approach of Ishida [67] have shown that the spin-orbit interaction splits up the IPS with $n = 1$ on Au(001). Namely the energy splitting is zero at $\mathbf{K} = 0$ and increases along the $\bar{\Gamma}\bar{X}$ direction being larger than 20 meV for $K = 0.25$ Å^{-1} [87].

Lifetimes of surface states

The study of lifetimes of excited electron (or hole below the Fermi level) states is very important in physics. Their knowledge allows one to ascertain the duration and the extent of the influence of an excitation and they are strictly related to the dynamics of charge and energy transfer and of screening including the effect of surface vibrations. For a free metal surface, even when the elastic lifetime is infinite, other effects are present, namely the electron-electron interaction (inelastic lifetime) and the phonon one (vibrational lifetime). The former phenomenon leads to lower energy surface or bulk electrons together with the creation of an electron-hole pair. A nice schematic picture of such processes for the Shockley state on Cu(111) and Cu (001) and IP bands is provided by Fig. 1 of [88]. While ARPES is limited to measuring lifetimes of hole states, scanning tunneling spectroscopy (STS) can explore those of states above and below the Fermi level. The interaction of an electron with the metal bands is described by the GW method using the Random Phase Approximation or by TDDFT [89] Results for the lifetimes, τ, of the (111) face of noble metals worked out by theory including the phonon contribution and STS experiments were found in excellent agreement. For Cu(111) at the band edge of the Shockley state both theory and experiments predict $\tau \approx 21$ meV [90].

Recent results for organic adsorbates

Since forty years several investigations have dealt with the modification of surface states by adsorption [91, 92, 93]. In this review we concentrate on very recent results regarding the effects of adsorption of organic molecules on surface states. To obtain a thorough understanding of the properties of the interface between an organic semiconductor and a metal research has addressed by 2PP experiments the electronic states of HBC (hexa-catahexabenzocoronene), a promising photovoltaic material, on Cu(111) [94]. It is shown by increasing the coverage Θ from 0 to 2 Monolayers (ML) the Shockley state is quenched and the work function Φ of the HBC/Cu system decreases due to a combination of push back and electron transfer. New states appear at larger HBC coverage and are interpreted as IPS modified by the molecular layer on the metal. An interesting behaviour of the Shockley state is found for NTCDA (1,4,5,8-naphtalene tetracarboxylic dianhydride) on Au(111) [95] It is known that by deposition of a low amount of alkali atoms (Na) on noble metals an increase of the binding energy of the Shockley band occurs. The Shockley state is also sensitive to the presence of an organic film which displaces it upwards. In [95] the two effects are combined. First one covers Au(111) with a small amount of Na shifting down the Shockley state and then deposit a monolayer of NTCDA: the Shockley state modi-

fies its energy which appears very similar to that on clean Au(111) and suggests a very weak interaction between NTCDA and the metal. So this work outlines the importance of the behaviour of Shockley states and the effect of alkali adatoms in controlling organic molecule adsorption and charge transfer. Among a variety applications scanning tunneling microscopy (STM) has demonstrated to be able to induce non local manipulations leading to molecular desorption [96]. The experiment considered cloro-benzene molecules on Si(111)-(7×7) and showed that charge injection from an STM tip with positive voltage V can cause molecular desorption, once V reaches the desorption threshold. The effect decreases exponentially ($\simeq 100$ Å) from the location of the injected charge. From the electronic point of view charge is transferred from the STM tip to a new surface state predominantly located at faulted rest and unfaulted rest atoms which is the threshold surface state for nonlocal desorption and hints new ways of long range surface manipulation via surface states [97].

1.4 Adsorption of simple atoms and molecules

Adsorption is a phenomenon by which the surface of a solid links molecules from a gas or a liquid. It is generally a sponteneous one which is accompanied by a decrease of the free energy of the system and of entropy. The process is exothermic and the released heat is called is heat of adsorption. Chemical adsorption or chemisorption requires a higher production of heat and often need to overcome a barrier of activation energy. Physical adsorption or physisorption always occurs and asks for a lower energy of adsorption. Chemisorption does not always occur, but couples to physisoption when the molecules are closer to the surface and chemical bonds are formed.

The variety of adsorption phenomena, the possibility of covering only a small fraction of the solid surface (in percentage), a full layer or overlayer, from few to several layers, the enormous amount of different adsorbates from the simplest, hydrogen, to molecules with hundreds of atoms opens up an incredible number of new effects. This somewhat limits our treatment to prototypes of the main classes of adsorption.

1.4.1 Chemisorption of simple atoms and molecules

The modern age of chemisorption started with Grimley [98] and later Grimley [99] and Newns [100] who independently adapted the Anderson model for magnetic impurities to chemisorption. They pointed out that the energy of an orbital of a chemisorbed atom is equal to $\varepsilon_{A\pm\sigma} = E_A + J_A n_{A\mp\sigma}$, where J_A is the Coulomb repulsion. So the effective energy of an orbital depends on its occupancy by an electron opposite spin. Contrarily the occupancy of an orbital $n_{A\pm\sigma}$ depends on the distance of an orbital of opposite spin $\varepsilon_{A\mp\sigma}$ from the Fermi level. This indeed shows that chemisorption cannot be treated in a one electron picture. We have seen how DFT progressed to supply a realistic tool to calculate the energetic and often with the help of experimental data the exact position of adsorbed molecules also with several atoms. Following Grimley and Newns, Hammer and Norksov [101] provided simple models to interpret the results by DFT which well account for the main trends of chemisorption and in which a fundamental role is played by the local density of states (LDOS). Take

oxygen chemisorption on metals. We can imagine that this process occurs in two steps. First the adsorbate $2p$ state interact with the wide sp metal band and causes a single resonance. Its interaction with the narrower d band (strong coupling in the Grimely-Newns's model) splits it into two states: one bonding and the other one antibonding, below and above the d band, respectively. The adsorption energy can be written as $E_{ads} = E_0 + E_{hybr}$. Although the larger energy is the sp contribution, this is practically constant for all metals while the second term allows distinguishing between different values of adsorption energy. In the case of Cu, Ag, and Au the antibonding band is completely filled and repulsive, while if we move on the left of the periodic table the anti-bonding state becomes depopulated as the d band shifts upwards and chemisorpion becomes increasingly stronger:$\simeq -0.6$ eV (Ag); $\simeq -0.9$ eV (Pd); $\simeq -2.8$ eV (Ru); $\simeq -3.5$ eV (Tc); $\simeq -4.00$ eV (Mb); -4.2 eV (Nb), with the d band centre roughly increasing from -4.0 eV to 2.0 eV, correspondingly.

To examine the molecular adsorption consider as a benchmark system the adsorption of CO. Experimental and theoretical studies suggest that electron donation from the CO 5σ filled orbital to the sp and d bands and backdonation from these bands to the 5π empty orbital is mainly the origin of this chemisorption phenomenon. The interaction with the sp band of the metals determine a downshift and broadening of 5σ and $2\pi^*$ orbitals, and with the d band, two bonding and two anti-bonding states below and above the pristine states. In conclusion the d band contribution to the adsorption energy E_{d-ads} can be expressed in the form of a hybridization gain for the 5σ orbital and an orthogonalization cost for the 2π one. Analogously to oxygen if we move from noble metals to the right of the periodic table we span from dissociated CO (from Ag to Rh) to about -3.0 eV CO chemisorption for Nd. Finally observe that this behaviour on the periodic table is fairly general.

Another fundamental question in chemisorption regards bond-making and breaking. For H dissociation bonding and antibonding states similar to atomic adsorption display a bond which is a little stretched. In this case a bonding and anti-bonding states similarly to atomic adsorption occur, while for stretched bonds the electronic structure of the molecule is alike that of the final state.

Very recently a sophisticated calculation has been provided by L. Schimka et al., who have abandoned the most recent functionals for alternative methods based on the many-electron approach, the random phase approximation (RPA) [51]. In fact even for a small molecules like CO on Pt(111) the usual semilocal functionals tend to overestimate chemisorption energy and not provide the correct the correct monoxide site. When exact Hartee-Fock exchange is combined with RPA we observe that the adsorption energy decreases which is due to interaction of the two frontier orbitals of CO, the 5σ and the $2\pi^*$ with the metal states. The 5σ orbitals are partially filled above ε_F determining a strong interaction in the atop site. The RPA also restores the correct order in energy for the most critical cases lowering the binding energy of 350-550 meV: -0.42 eV (adsorbed on Cu(111) in the top site) < -0.32 eV (Cu, face centered cubic site, fcc); -1.31 eV (Pt top) < -1.23 eV (Pt fcc); and -1.43 eV (Rh top) < -1.28 eV (Rh, hexagonal close packed, hcp). Another example is benzene on ferromagnetic Ni(111). In the RPA the experimentally observed hollow site is favoured while the total adsorption energy is instead lowered by RPA (-0.95 meV) compared to PBE (-0.65 meV) owing to a strong van der Waals bond.

Alkali atoms on metals

Among atomic adsorbates, alkali metal adsorbed on metal surfaces have been subject of intense investigations in order to clarify fundamental issues in adsorption phenomena, as well as for their technological relevance as workfunction modifiers and surface dopants. Early description of these prototypical system dates to about 80 years ago with the Langmuir-Gurney model [102, 103]. The knowledge on this apparently simple system have remarkably improved during the last three decades showing the occurrence of various non-trivial phenomena overcoming such model, as reviewed by several authors in the past [104, 105] and more recently [106].

One example of peculiar phenomena lies in the correlated "vertical diffusion" motion observed for Na atoms on copper. Measurements of surface diffusion based on helium atom scattering for Na/Cu(001) have proven unable to explain an observed coverage dependence of the 2D motion [107]. By high resolution ^{3}He spin-echo, Alexandrowicz et al., [108] could demonstrate that experimental findings are accurately reproduced upon introducing an explicit dependence of the Na coordinate on the local adsorbate concentration, that is a time-dependent quantity at finite temperature, hence leading to a confined motion also along the surface normal, occurring on the same timescale as the diffusive motion. However, a coverage dependence of the Na-surface bondlength is not expected [105]. DFT simulations [109] could eventually clarify this puzzle demonstrating that, while the Na-Cu bond is minimally affected by adsorbate concentration, the extent of the electronic density towards vacuum is modified considerably because of the dipole electric field induced by the other adsorbates. Being the adsorbate distribution inhomogeneous and time-dependent, this translates in a time evolution of the turning point for the scattered probe atoms. Related (yet static) electronic effects occur in emphasizing the corrugation of quasi-1D structures observed by Helium atom scattering (HAS) for Li and Na on Cu(001) as coverage approaches saturation, where changes in the atomic height are irrelevant. We will return to this case when discussing adsorption dipoles (Sect. 1.5.2).

Alkali atoms are also prototypical effects for the study of surface diffusion phenomena. Considering again Na on copper, the effect of step on surface diffusion have been studied by adopting a vicinal Cu(115) surface [110]. Motion is anisotropic and occurs prevalently parallel to the step edges, following intuition. Additionally, Na-Na collective effects described above are also anisotropic, pointing to a screened interaction for adsorbates on different terraces.

1.4.2 Physisorption of noble gases on metals

Adsorption of noble gases is for several reasons an important topic in surface science. Already about fifty years ago Scoles [111] and Boato [112] performed the first experiments of diffraction of light noble atoms on solid surfaces. This technique has been extensively applied by Toennies [113] and other scientists to obtain detailed dispersion relationship of phonons on several surfaces. More recently Allison has employed beams of the fermion isotope ^{3}He to check the diffusion of alkali adatoms (see previous chapter) [114]. Ar, Kr and Xe have been used for microscopic tribological models for perspective technological applications.

Being atoms with a closed shell systems, noble gases interact with a surface mainly with van der Waals or London dispersion forces by instantaneous dipoles. For this reason their bond to the surface is a physisorption one where we have already observed that DFT with semilocal corrections is not sufficient. The weakness of the interaction between the atom and the surface introduces the main complication since the adsorption energy is strongly dependent on correlation so that a local (semi-local) qualitative estimate, sufficient at shorter distances for a chemical bond, is insufficient to yield van dew Waals energies, in which the polarizability of the probe and the long wavelength dielectric constant are missing. Still LDA/GGA DFT treatments have supplied important information. A general property, validated by GGA-DFT, independent of the functional, is that the equilibrium distance from the surface increases from Xe to Ar and it correlates with the adsorption energy that vary from few meV for He to $-320/-360$ meV for the heaviest one, Xe. The results of Da Silva and Stampf [115], confirmed by low energy electron diffraction (LEED) measurements, found that Xe adatoms preferentially bind to low coordination top sites instead to the highly coordinated hollow sites on metals because when charges of the atom and of the metal begin to overlap, Pauli repulsion is present and electrons are transfered more easily from on top sites to hollow ones getting the atom closer on top. Non-local vdW DF functionals showed later that the hollow sites for Xe are maxima and the atop site a true minimum [51]. This phenomenon hold for closed packed surfaces, i.e., Pt(111), Pd(111), Cu(111) for Xe. However, a potential curve of a noble gas atom is erroneous when calculated by GGA-DFT. It is clear that a many-body seamless solution, as a function of distance from the surface, would be desirable for correct results.

A more subtle effect of He interacting with transition metals surfaces and the Cu(111) one, is the so called anti-corrugating effect. In fact elastic scattering measurements of He performed by Rieder [116] on Rh(110) and Ni(110) showed unexpected features in full disagreement with intuition. In order to explain their data, these authors assumed that the corrugation profile seen by He is off phase with respect to the surface lattice atom positions and that the classical turning point of the interaction potential is farther away at the short bridge position than at the top one, for a fixed kinetic energy of the impinging atom. GGA-DFT calculations by Scheffler's group [117], which produce reasonable results at this atom-surface distance since the He-suface-potential is in its repulsive part, show that the property of s for He and p for Ne wavefunction facing the d metal ones at top and bridge position determine the anti-corrugating effect. In a later paper on Cu(111) anticorrugation, which explains very satisfactorily the anomalies of phonon spectra, was accounted for in terms of the relative kinetic energy ΔK of the electrons between top and bridge sites for the same impinging He kinetic energy. In other words $\Delta K(\text{Bridge}) > \Delta K(\text{Top})$ and overcomes the electrostatic difference $\Delta U(\text{Top}) > \Delta U(\text{Bridge})$, being the exchange correlation term negligible. On the hand for a simple metal He/Al(111) the standard corrugation is observed and $\Delta K(\text{Bridge}) < \Delta K(\text{top})$ [118].

Surface properties studied by adsorption phenomena

While the emphasis of adsorption studies may be more frequently on the adsorbate, absorption and diffusion phenomena are also a tool to investigate surface properties. One obvious example is given by atom scattering experiments. We would also like to mention a less direct example, where the observed atomic diffusion at a surface can be linked to the substrate approaching a structural transition [119]. Bulk cobalt is characterized by a hexagonal close packed structure at ambient temperature and pressure, but thin Co films can be stabilized epitaxially on top of Fe(001) which acts as a template with square symmetry. Hence, a metastable body-centered-tetragonal structure is obtained up to about 10 Co layers (after which the film transforms into hcp crystallites). Despite the atomistic structure of the surface keeps unaltered, the diffusivity of Co adatoms has been shown to depend dramatically on film thickness: the process gradually evolves from an activated one, with a barrier of about half an eV on clean Fe(001), to being practically barrier-less already at a thickness of 5 ML. Experimentally, this was determined by a statistical analysis of Co island size distributions, from which the diffusion coefficient is extracted, as a function of thickness and temperature. Density functional theory simulations have then identified the transition state in the diffusion mechanism as a Co adatom occupying the bridge site, and that such site is stabilized by deformations in the substrate that increase in magnitude with film thickness. These deformations locally recover a structure in closer resemblance to the hexagonal one, so their energy cost drops to zero as the film approaches the structural transition.

1.5 Adsorption of organic molecules

The flexibility offered by natural and synthetic organic chemistry leads to enormous possible choices in the choice of organic adsorbates. Example of classes of molecules having attracted significant interest in the literature for fundamental aspects and applications are self-assembled monolayers (SAM), porphyrins, and policyclic aromatic hydrocarbons (PAH). Although the definition strictly applies to a wide class of molecules, with the SAM acronym one customarily denotes a specific class of self assembled adsorbates where molecules are composed by a chemisorbed head group, a tail, and a functional termination. A prototypical case consists of n-alkanethiols where the anchoring group is a sulfur atom and the tail a $(\text{-CH}_2\text{-})_n$ chain, but many more configurations are possible [120]. This molecules find various applications in surface coatings. Porphyrins are molecules with enormous significance in biology and interesting catalytic properties. They can incorporate different metal centers which can be adjusted for tailored applications, and their properties and functionalities are characteristically influenced by interfacial interactions [121, 122].

Policyclic aromatic hydrocarbons have attracted significant interest for organic electronic devices [123]. In the following we will focus on this latter subset to select few test cases for additional discussion.

1.5.1 Aromatic molecules on semiconductors and metals: configurations, electronic and spectroscopic properties, π and σ bands

Pentacene on TiO_2

The performances of electronic devices depend on a diversity of factors, including the structural, electronic, and spectroscopic properties of the very first layer of molecules at the hybrid interfaces within the device. The arrangement of the first molecules may steer the crystalline ordered growth of an organic active layer,[124] which is especially important since high quality of the organic crystal is required [125]. Also, the mobility within organic materials, also when high molecular ordering can be achieved, is optimal only at the directions that maximizes intermolecular couplings [126]. Additionally, the ultimate transfer at a contact depend on the overlap of the molecular wavefunctions with the substrate ones.

An especially interesting and prototypical case that we take here as an example is constituted by pentacene ($C_{22}H_{14}$). This aromatic hydrocarbon is characterized by very high hole and electron mobility [127, 128] that exceed that of amorphous silicon. The adsorption of pentacene on different substrates has therefore been widely studied both experimentally and theoretically. We select here few examples to describe how different levels of interaction influence the growth.

The anisotropy of a weakly interacting substrate has proven effective to gently influence the molecular adsorbates, without affecting too strongly their electronic and spectroscopic properties. One such example is the case of pentacene on the rutile $TiO_2(110)$ surface. This surface is characterized by the formation of rows of protruding O atoms along the [001] crystal azimuth; rows are spaced about 6.5 Å along $[1\bar{1}0]$ and atoms protrude by about 1 Å with respect to surface Ti [129] [130], forming an ideal template to accommodate planar molecules as found for pentacene (other examples are perylene and its derivatives [131]. Submonolayer phases of pentacene on $TiO_2(110)$ have been studied by STM, HAS, and near edge X-ray absorption fine structure (NEXAFS). These experiments have demonstrated the formation of a very ordered phase [132] with molecules adsorbed in a nearly planar geometry (tilt angle $\approx 25°$) and aligning along the $[1\bar{1}0]$ crystal azimuth with intermolecular distance dictated by coverage, and approaching that of the organic crystal at monolayer completion. In the other surface azimuth ([001]) intermolecular π-π attraction stabilizes stripes of pentacene. The NEXAFS spectrum of these molecules is reported in Fig. 1.4a for the gas phase (calculations shown as a reference) and in Fig. 1.4b for pentacene/TiO_2. It exhibits several characteristics testifying that the interaction with the substrate, although sufficiently strong as to drive the ordered phase, has only a minor influence on the molecular orbitals: molecular features are clearly resolved, not showing an hybridization-induced broadening present in other cases (see the other panels, discussed below); the spectra at monolayer coverage already resemble those of a thin overlayer and, once spherically averaged, gas phase ones [133]. The ordered phase allows unprecedented analysis of the symmetry of the molecular orbitals that is only possible for stabilized molecules, and that is fully rationalized by theoretical simulations of the spectra based on the transition-potential approach [134] (see

Fig. 1.4a). One can identify the first unoccupied resonances as due to transitions to final bound states (LUMO, LUMO+1 and higher states) having π symmetry. For final unbound states ≈ 5 eV higher energy than that threshold, transitions to σ states emerge. Given the asymmetry of pentacene and the uneven length of its C-C bonds, the energy of σ states differ according to the dominant contribution of in-plane orbitals along the long or short molecular axis. Such an effect identifies an azimuthal dichroism in the spectra that can be used to resolve in-plane molecular orientation by NEXAFS, as was done to validate a model of perylene ($C_{20}H_{12}$) adsorption on the same surface, with the molecular axis along $[1\bar{1}0]$ where a rounded appearance of the molecules in the STM images could not be conclusive [131].

Pentacene on Silicon

The case of pentacene on silicon surfaces exhibits a completely different behavior. On this semiconductor, the molecule is found to strongly chemisorb. Several studies have highlighted possible configurations on Si(001)-(2×1). A work by the Yates group [137] combined STM with slab simulations at the PW91 level revisited previous assignments and pointed out the formation of six to height Si-C covalent chemical bonds, and an adsorption energy of up to 128 kcal/mol. This is realized for a nearly flat molecule bridging between adjacent rows of Si dimers. Other configurations include strongly distorted pentacene with sp_3 hybridized C atoms. Consequently, a NEXAFS spectrum of pentacene on Si(001)-(2×1) reveals lost conjugation and missing contributions by peripheral C atoms at the otherwise expected $1s \rightarrow$LUMO transition energy [138]. Chemisorption also occurs on Si(111)-(7×7). This strong interaction of pentacene with a silicon surface can be reduced by passivating the substrate with H [139] or by organic adsorbate functionalization [140].

Pentacene on noble metals

Adsorption of pentacene on metal surfaces also raised significant interest because of the occurrence of organic/inorganic interfaces at potential contacts. Among the noble metal surfaces, Au(111) is supposedly the one exhibiting the smallest interaction with the adsorbate. There, pentacene adsorb mostly planar; however, the interaction is still appreciable in inducing a weak bending of the molecule [141]. On Au(110) [135] different structures are observed: a (3×6) one, Fig. 1.4c, with planar molecules having their long axis along [001], exhibiting a significant broadening of the LUMO peaks and significantly smaller azimuthal dichroism than the one of free molecules. At higher coverage, a (6×8) structure where planar molecules coexist with ones having the long axis along the surface normal. The spectra of the two intermixed phases can be distinguished thanks to a different dependence on the experimental geometry in Fig. 1.4d. For example, π transitions are excited with $E \parallel [110]$ for flat-lying molecules and $E \parallel [001]$ for standing ones. Their comparison at about 285 eV in panel d testifies the dependence on adsorption angle of the electronic coupling of the π system with the substrate orbitals, with standing molecules leading to better resolved features and larger azimuthal dichroism. By increasing the interaction strength, silver and copper surfaces also present mostly planar molecules, with upwards bending

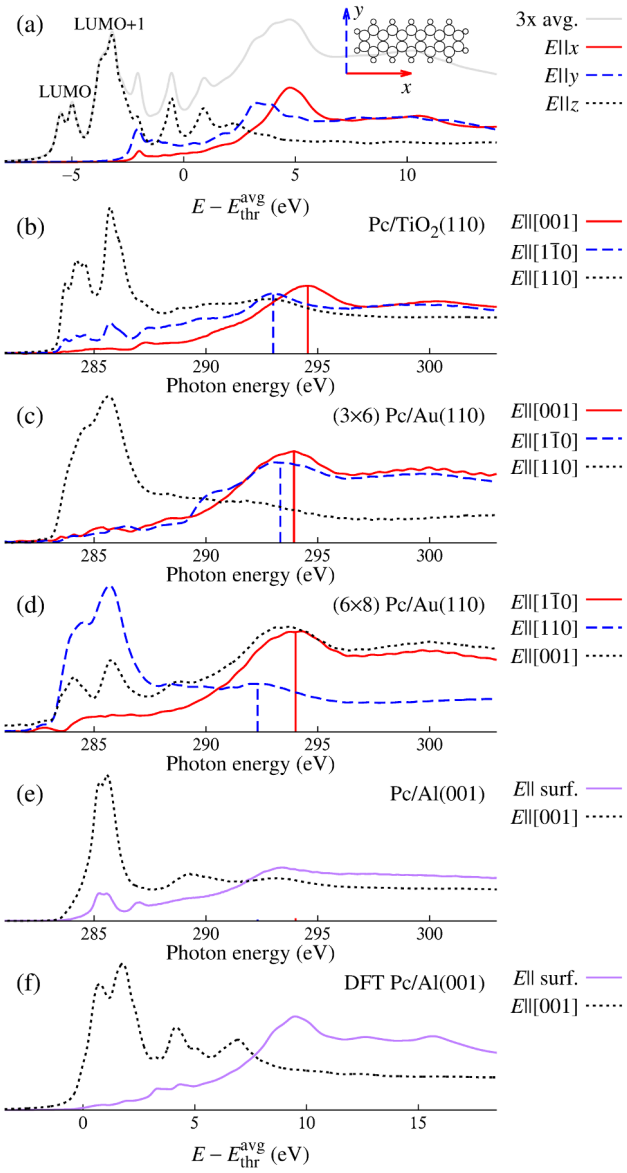

Figure 1.4: NEXAFS spectrum of pentacene: (a) theoretical result for the gas phase [134]; (b) measured on TiO_2 [132]; (c)-(d) measured on Au(110) [135]; (e) measured and (f) computed for pentacene on Al(001) [136].

of the molecule along its short axis. The mixing of the molecular and substrate electronic states becomes more relevant, featuring the filling of the lowest unoccupied molecular orbital on Ag(111) [142], Ag(110) [143], Cu(111) [144], Cu(001) [145], and Cu(110) [146]. Consequences of the LUMO filling are the possibility to detect such orbital in photoemission experiments normally accessing the molecular states up to the highest occupied molecular orbital (HOMO) [143], and their reduced intensity or disappearance in NEXAFS.

Pentacene on Aluminum

As another metal of interest for device research, aluminum presents a stronger interaction that opens to a peculiar scenario. The adsorption of pentacene on Al(001) was studied by a combination of experimental and theoretical techniques [136]. It was found by reflection high-energy electron diffraction (RHEED) and STM that adsorption induces a reconstruction on the substrate, that appears as a rippling of Al rows along [100] having a corrugation of 30 pm in the STM taken in exposed surface areas. The periodicity of these rows across $[1\bar{1}0]$ is 1.6 nm, the same as molecular stripes also identified in STM that extend along [100] with molecules having the long axis along [110]. From the theoretical point of view, the adsorption is somewhat intermediate between chemisorption and physisorption. If a DFT description with a semilocal functional is used, molecules are barely bound with GGA, whereas an adsorption energy of ≈ 2 eV is obtained with LDA showing an upward curvature (similarly to Cu adsorption) [147]. The inclusion of van der Waals correction, there at the Grimme level, has a major impact on the GGA results. Of the possible adsorption sites compatible with the experimental orientation, all of them but one still present a mostly flat molecule with adsorption energy up to 1.50 eV. The other one, which is centered on a bridge site with the central C atoms on top of two Al atoms, is the most stable with an energy of 2.20 eV and features a V-shaped molecule. This configuration is depicted in Fig. 1.5 and is characterized by a V-angle at the center of 155° and a difference in C heights of 1.35 Å, with a deformation that costs, in the gas phase, an energy of 1.35 eV. This structure is stabilized by the optimal matching of the central C atoms with two Al ones, with a C-Al distance as small as 2.20 Å. This is only made possible, however, by the inclusion of dispersion forces: these allow a shorter distance between the aromatic rings and the surface, eventually allowing for the direct C-Al anchoring. Spectroscopic and microscopic properties simulated for molecules adsorbed in the V-shaped are in very good agreement with the observations and corroborate this results. In particular, NEXAFS spectra reported in Fig. 1.4e (experiments) show the molecules to lie mostly planar, with an effective tilt angle of the aromatic planes of $28 \pm 5°$ with respect to the surface, that takes into account molecular deformation and defect sites. Given the hybridization with metal states, a broadening of the molecular features could be expected similarly to the case of pentacene on Au(110). Differently from the gas phase, the signature of transitions to π^* orbitals is much narrower both in measured and computed (Fig. 1.4f) spectra, suggesting also in this case that filling of the LUMO takes place hence removing it from the unoccupied manifold of possible final states.

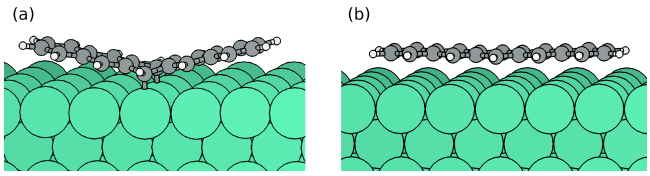

Figure 1.5: Adsorption configuration of pentacene on Al(001) [136]. (a) Most stable V-shaped configuration in the bridge site. (b) Flat-lying on a top site. Balls of increasing size denote H, C, and Al atoms.

Band symmetry and spectroscopy

An effective tool for a rational analysis of spectra of adsorbed molecules is the identification of the molecular energy levels in the DOS and surface band structure of the system (see Fig. 1.3 for an example of a clean substrate). To this respect, many ab initio codes implement the possibility to project the surface bands onto the molecular eigenstates, typically computed by a separate calculation for the free molecule. As a result, one can visualize "fat bands", where the color or size of the symbols in the "spaghetti plot" is proportional to the molecular contribution. Alternatively, a **K**-resolved DOS (projected onto molecular orbitals) can be used and possibly superimposed as a color map on the usual surface band plot. The two approaches are conceptually equivalent and while the former may be more convenient to represent regions where only few bands appear, the latter is advantageous for high density of states and is the natural framework to describe the continuous spectrum of an extended substrate. The **K**-resolved DOS is reported in Fig. 1.6 for thymine molecules forming rows of π-stacked molecules deposited on Si(001) [148]. In this case, the dispersion of HOMO- and LUMO-derived states (see insets) can be identified, allowing the distinction of molecular features and molecule-induced substrate ones in optical reflectance spectra.

1.5.2 Adsorption-induced charge rearrangements / induced dipoles / induced spin distributions.

Induced charge rearrangements

Out of the various adsorption induced phenomena, such as substrate relaxations, reconstructions, surfactant effects, etc., one of the most relevant and possibly easily visualized is the displacement of the electron density of the combined system when that of the summed fragments is taken as a reference. That quantity, $\Delta\rho_{\rm ads} = \rho_{\rm mol/surf} - \rho^{\rm gas}_{\rm mol} - \rho^{\rm clean}_{\rm surf}$, is in principle exactly accessible by DFT where $\rho_{\rm mol/surf}$, $\rho^{\rm gas}_{\rm mol}$, and $\rho^{\rm clean}_{\rm surf}$ are the ground state charge densities of the full system, of the free molecule, and of the clean substrate, respectively (the latter two commonly taken at the same coordinates they attain upon adsorption).

Let us take again as an example the case of adsorbed pentacene. A strong electronic charge reorganization at the interface occurs for various metals, see, e.g.,

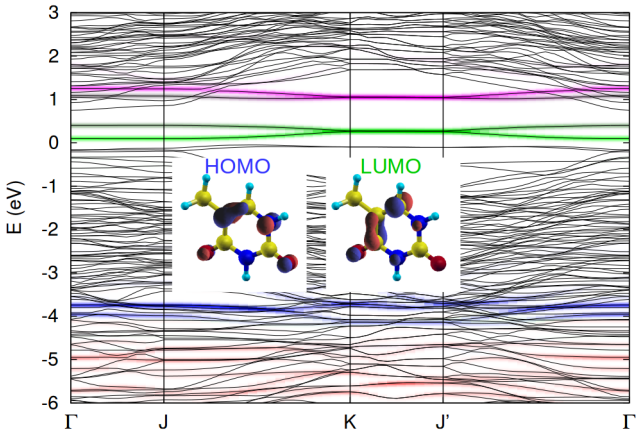

Figure 1.6: Surface band structure of thymine molecules on Si(001) in the "dimer-bridge" configuration at half coverage [148] with molecular contributions shown as a the color map of the **K**-resolved DOS. HOMO and LUMO of gas phase thymine are shown in the insets.

Ref. [146] (also recall the filling of the LUMO of pentacene on a variety of substrates as presented in Sec. 1.5.1). The case of pentacene on Al(001) may serve as a tool to identify the relation between adsorption configurations and different charge displacements. To that purpose, in Fig. 1.7 the quantity $\Delta\rho_{\rm ads}$ is reported for the two configurations, B chemisorbing with a V-shape (Fig. 1.7a-b) and T physisorbing nearly planar (Fig. 1.7c). Red colour indicates regions of higher electron density and blue ones of lower density. By plotting in Fig. 1.7a the isosurfaces corresponding to an isovalue of $\pm 0.04e/\text{Å}^3$, accumulation of electron density in the C-Al bond formed at the center of the molecule can be seen. A corresponding charge depletion is instead observed in the vicinity of that bond at a smaller isovalue ($\pm 0.01e/\text{Å}^3$) in Fig. 1.7b. The net electron transfer from Al to the molecular region was estimated to amount to $0.56e$ [149]. To visualize any effect of electron density rearrangement in the physisorbed case, one has to take a lower isovalue $0.005e/\text{Å}^3$ in Fig. 1.7c.

Induced dipoles

In relating the adsorption density rearrangements to workfunction changes one is tempted to express the dipole moment per adsorbed species at a given coverage as the product of the displaced charge (as estimated by Bader or related approaches) times an adsorption distance. However, as pointed out by Bagus and coworkers [150], several and often canceling terms contribute to the interface dipole so that the above expression is only formally valid. So one may have negatively charged adsorbates, like I/Cu(111), that decrease the surface workfunction contrary to expectations.

Also in the most simple and prototypical case of alkali atoms on a metal, several interesting phenomena may emerge.

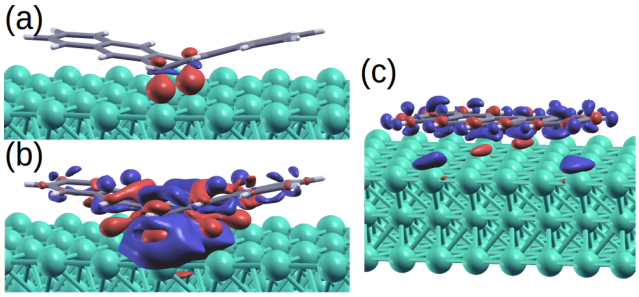

Figure 1.7: Adsorption charge of pentacene on Al(001). (a) and (b) Pentacene on the bridge site, showing surfaces at adsorption charge isovalues of (a) $\pm 0.04e/\text{Å}^3$ and (b) $\pm 0.01e/\text{Å}^3$. (c) Pentacene on the top site, with isovalues of $\pm 0.005e/\text{Å}^3$.

For example, the charge displacement induced by adsorption of Cs on Cu(001) is depicted in Fig. 1.8a where we subtract from the electron density of the full system that of neutral Cs and of clean Cu(001). The first and more obvious feature is the transfer of electrons from the Cs region (diffuse red region centered at Cs) to the metal (see the blue region mostly located just above the surface layer). However, one can also appreciate: a localized polarization around the nearest Cu atoms that goes beyond earlier treatments by the jellium model [69]; a charge displacement in the region closer to the Cs nucleus, with negative/positive charge at larger/smaller distances, hence producing a dipole moment opposite to the total one. The latter effect corresponds to the polarization of the inner shell and reduces the total dipole moment especially for the heavier alkalis (by 11% for Cs, reducing dipole-dipole repulsions by 20%). The total dipole moment, as computed by DFT-PBE [151], produces a variation of the workfunction that at 0.06 ML coverage amounts to 1.97 eV, in excellent agreement with the measured value of 2.0 eV [152]. Lighter alkalis show qualitatively similar results, although reduced in magnitude [151].

It is noted that the surface dipole is a determined self-consistently. In particular, the experimental saturation of the workfunction change at a given coverage demonstrates the coverage dependence of the adsorption dipole as the overlayer is increasingly denser. Inhomogeneous changes in the local adsorbate density, while keeping the total coverage constant, also lead to interesting phenomena. For example, the dipole-dipole repulsion of adsorbed Na atom pairs on Cu(001) is modified from a pure R^{-3} law (R being the Na-Na distance) because of the reduction of the dipole moment as they come closer: neglecting this effect overestimates the repulsion energy by 20 meV when Na atoms are two Cu unit cells apart [153]. Reduction in the adsorption dipole induced by local density increases contribute to the stability of quasi-1D structures observed and computed for Li/Cu(001) [154, 155] and Na/Cu(001) [156, 157] as saturation coverage is approached. Atom scattering experiments demonstrate a 1D corrugation of the probe-surface interaction that, linked to the surface electron density through the effective medium theory, is actually due to larger extension of the density towards vacuum, as the workfunction is locally reduced because of the

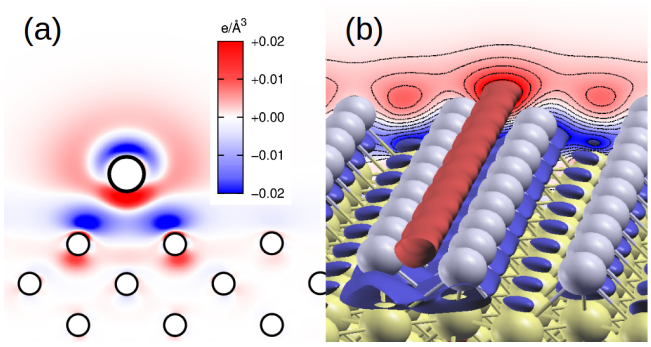

Figure 1.8: (a) Side view of the adsorption charge for Cs/Cu(001). Large and small circles mark the position of Cs and Cu atoms, respectively. (b) Charge redistribution in forming 0.6ML structures of Li/Cu(001), as compared to the individually adsorbed Li atoms. Red regions mark increased electron density. Isosurfaces are depicted at ± 0.01 Å^{-3}.

increased density of dipoles. As an example, the electron density displacement for an high-coverage structure of Li/Cu(001) [155] is reported in Fig. 1.8b, where we show the difference between the adsorption charge density $\Delta\rho_{\rm ads}$ for the full structure and a reference adsorption charge calculated by summing independent contributions by individual Li atoms at lower coverage. The accumulation of electron density in the red "pipe"-shaped region, probed by the experiments, indicates depolarization of the alkali-surface bond (see the blue region underneath) in favor of a metallic-like bond within Li atoms.

Induced spin distributions

Adsorption phenomena also have an interplay with spin-dependent phenomena. Cases of magnetic substrates where molecules can attain magnetic properties as a consequence of hybridization are reported (see, e.g., C_{60}/Fe_3O_4 [158] or pentacene on Co islands on copper [159]) or, conversely, ones of adsorbed magnetic molecules (e.g., porphyrines incorporating magnetic centers). The combination of a magnetic molecule with magnetic substrates [160] also raises significant interest for molecular spintronic devices.

However, it is intriguing to observe that adsorption can induce spin-polarization also for non-magnetic molecules on non-magnetic substrates. A case that has attracted particular interest is the one of covalent adsorption on graphene. Perfect clean graphene is spin-compensated and several techniques have been proposed to induce magnetic moment. Casolo and coworkers [161] already demonstrated that the adsorption of an H atom induces a net magnetic moment of 1 $\mu_{\rm B}$ by effectively removing one p_z orbital from the π band of graphene: that, by Lieb's theorem for bipartite lattices, translates in the observed magnetism. The unpaired electron occupies a spin-polarized state (called "mid-gap state") occurring right at the Dirac cone which is localized in space around the adsorbate given the vanishing substrate

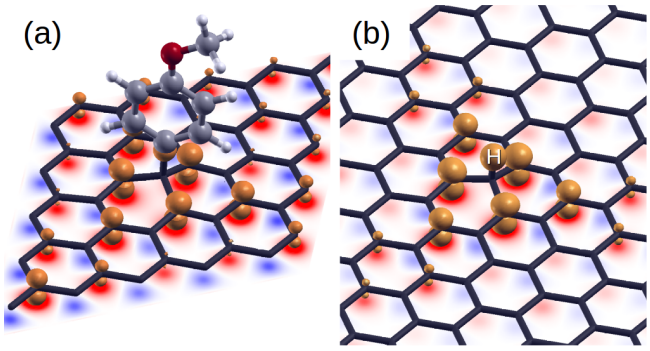

Figure 1.9: Electron spin density $n_\uparrow - n_\downarrow$ for (a) methoxybenzene and (b) hydrogen adsorbed on graphene. The red isosurface correspond to the value of 0.05 eÅ^{-3}. Red and blue shades underneath are a false color plot for values cut through a plane passing 0.65 Å below graphene and saturate at ± 0.02 eÅ^{-3}.

density of states, although periodic calculations show the appearance of bands in a small, size-dependent, energy gap. Being this effect intimately related to modifications in the graphene lattice, rather than on the properties of the adsorbate, and was therefore extended to more general cases of covalently bonded organic molecules on graphene [162, 163] and carbon nanotubes [164]. The interested reader is referred to the review by Martinazzo for more details [165].

We recall few experimental facts. Observations of individual atoms and molecules on graphene are possible by the transmission electron microscope [166]. Hydrogen adsorption can be used to open a highly demanded band gap, as shown for H/graphene/Ir(111) [167]. Also, at low coverage hydrogen can induce a three-order-of-magnitude enhancement of the spin-orbit interaction in graphene [168]. Eventually, magnetic properties for organically functionalized graphene samples have recently been measured showing the occurrence of antiferromagnetic domains [169].

The spin polarization of graphene with a covalent adsorbate is represented in Fig. 1.9 where we report the spin density $n_\uparrow - n_\downarrow$ for an adsorbed molecule (methoxybenzene, $CH_3OC_6H_5$) and atomic hydrogen, the latter computed for a larger (10×10 unit cell). We start by describing the case of anisole [163] in Fig. 1.9a. Upon covalent adsorption on a C atom named C_0 belonging to one sublattice (A), that atom is lifted out of the carbon plane by 0.42 Å undergoing $sp_2 \to sp_3$ rehybridization. (This structural deformation costs 0.96 eV, that are subtracted from the adsorption energy leading a final energy gain of only 0.32 eV despite the additional C-C bond.) The occupied midgap state is only minimally contributed directly by the adsorbate. Rather, it is mostly located at the nearest C atoms of the other sublattice (B), as evidenced by the spin density. A smaller and opposite spin polarization at the A sublattice can also be identified. As anticipated, very similar findings occur for adsorbed H, that is presented as a comparison in Fig. 1.9b.

Ultrafast phenomena

We conclude this Section with the mention that adsorption induced charge rearrangements and spin distributions can exhibit ultrafast time dependence (on the femtosecond timescale) in response to excitations. As an example, the adsorption charge of a core-excited adsorbed molecule is altered so as to accommodate an additional electron. This results in specific decay channels in de-excitation spectra [170] that are explained in terms of a modified $\Delta\rho_{\mathrm{ads}}$ taking into account a filled LUMO orbital [72] injected from the substrate within few fs to screen the perturbation. Returning to covalently functionalized graphene, a core-level excitation in the adsorbate is shown to disrupt the adsorption induced magnetism on the fs time scale [171].

1.6 Conclusions

In this Chapter we have reviewed the main progresses in adsorption and band structures in the last years. Adsorption energies have benefited from increased computer power and from new functionals and van der Waals implementation. Nowadays accuracy of maximum 2-300 meV in bonding has been accomplished. For the surface bands a new area has opened up with the topic of adsorbed organic molecules. Especially with the help of synchrotron radiation methods and DFT approaches, the bands of organic adsorbates have been determined with great precision, including their orientation, tilting angle and the formation of metal-semiconductor overlayers of particular interest for organic electronic devices and photovoltaics. In this respect scanning tunneling microscopy and spectroscopy have also been of great help. New effects such as distance-surface manipulation of surface states have been foreseen.

Bibliography

[1] K. Burke: Perspective on Density Functional Theory, J. Chem. Phys. **136**, 150901 (2012)

[2] P. Hohenberg, W. Kohn: Inhomogeneous electron gas, Phys. Rev. **136**, B864 (1964)

[3] W. Kohn, L.J. Sham: Self-Consistent Equations Including Exchange and Correlation Effects, Phys. Rev. **140**, A1133 (1965)

[4] R.M. Dreizler, E.K.U. Gross: *Density Functional Theory*, 3 edn. (Springer-Verlag, Heidelberg 1990)

[5] J.P. Perdew, M. Levy: Comment on Significance of the highest occupied Kohn-Sham eigenvalue, Phys. Rev. B **56**, 16021 (1997)

[6] M.T. Yin, M.L. Cohen: Ground-state properties of diamond, Phys. Rev. B **24**, 6121 (1981)

[7] M.T. Yin, M.L. Cohen: Microscopic Theory of the Phase Transformation and Lattice Dynamics of Si, Phys. Rev. Lett **56**, 1044 (1980)

[8] G.P. Brivio, M.I. Trioni: The adiabatic molecule–metal surface interaction: Theoretical approaches., Rev. Mod. Phys. **71**, 231 (1999)

[9] J.P. Perdew, K. Burke, Y. Wang: Generalized gradient approximation for the exchange-correlation hole of a many-electron system, Phys. Rev. B **54**, 16533 (1996)

[10] S. Kummel, L. Kronik: Orbital-dependent density functionals: Theory and applications, Rev. Mod. Phys. **80**, 3 (2008)

[11] Y. Wang, J.P. Perdew: Spin scaling of the electron-gas correlation energy in the high-density limit, Phys. Rev. B **43**, 8911 (1991)

[12] W. Yang, J.P. Perdew: Correlation hole of the spin-polarized electron gas, with exact small-wave-vector and high-density scaling, Phys. Rev. B **43**, 13298 (1991)

[13] J.P. Perdew, Y. Wang: Accurate and simple analytic representation of the electron-gas correlation energy, Phys. Rev. B **45**, 13244 (1992)

[14] J.P. Perdew, J. A. Chevary, S. H. Vosko, K.A. Jackson, M.R. Pederson, D.J. Singh, C. Fiolhais: Atoms, molecules, solids, and surfaces: Applications of the generalized gradient approximation for exchange and correlation, Phys. Rev. B **46**, 6671 (1992)

[15] J.P. Perdew, H.Q. Tran, K.Burke, E.D. Smith: Stabilized jellium: Structureless pseudopotential model for the cohesive and surface properties of metals, Phys. Rev. B **42**, 11627 (1990)

[16] J.P. Perdew, K. Burke, M. Ernzerhof: Generalized gradient approximation made simple, Phys. Rev. Lett. **77**, 3865 – 3868 (1996)

[17] Y. Zhang, W. Yang: Comment on Generalized Gradient Approximation Made Simple", Phys. Rev. Lett **80**, 890 (1998)

[18] B. Hammer, L.B. Hansen, J.K. Nørskov: Improved adsorption energetics within density-functional theory using revised Perdew-Burke-Ernzerhof functionals, Phys. Rev. B **59**, 7413 (1999)

[19] J.P. Perdew, A. Zunger: Self-interaction correction to density-functional approximations for many-electron systems, Phys. Rev. B **23**, 3048 (1981)

[20] M. Cococcioni, S. De Gironcoli: Linear response approach to the calculation of the effective interaction parameters in the LDA+U method, Phys. Rev. B **71**, 035105 (2005)

[21] P. Garcia-Gonzalez, R.W. Godby: Many-Body GW Calculations of Ground-State Properties: Quasi-2D Electron Systems and van der Waals Forces, Phys. Rev. Lett. **88**, 056406 (2002)

[22] J.P. Perdew, M. Levy, J.L. Balduz Jr.: Density-Functional Theory for Fractional Particle Number: Derivative Discontinuities of the Energy, Phys. Rev. Lett. **49**, 1691 (1982)

[23] R. Parr, R.A. Donnell, M. Levy, W.E. Palke.: Electronegativity: The density functional viewpoint, J. Chem. Phys. **68**, 3801 (1978)

[24] S. Kummel, J.P. Perdew: Optimized effective potential made simple: Orbital functionals, orbital shifts, and the exact Kohn-Sham exchange potential, Phys. Rev B **68**, 035103 (2003)

[25] T.L. Gilber: Hohenberg-Kohn theorem for nonlocal external potentials, Phys. Rev B **12**, 2111 (1975)

[26] A.D. Becke: A new mixing of Hartree-Fock and local density-functional theories, J. Chem. Phys. **98**, 1372 (1993)

[27] A.D. Becke: Density-functional thermochemistry. III. The role of exact exchange, J. Chem. Phys. **98**, 5648 (1993)

[28] A.D. Becke: Density-functional exchange-energy approximation with correct asymptotic behavior, Phys. Rev. A **38**, 3098 (1988)

[29] C. Lee, W. Yang, R.G. Parr: Development of the Colle-Salvetti correlation-energy formula into a functional of the electron density, Phys. Rev. B **37**, 785 (1988)

[30] P.J. Stephens, F.J Devlin, C. F. Chabalowski, M.J. Fritsch: Ab Initio Calculation of Vibrational Absorption and Circular Dichroism Spectra Using Density Functional Force Fields, J. Phys. Chem. Lett. **98**, 11623 (1994)

[31] R.H. Hertwig, W. Koch: On the parameterization of the local correlation functional. What is Becke-3-LYP?, Chem. Phys. Lett. **268**, 345 (1997)

[32] V.N. Staroverov, G.E. Scuseria, J. Tao, J.P. Perdew: Comparative assessment of a new nonempirical density functional: Molecules and hydrogen-bonded complexes., J. Chem. Phys. **19**, 12129 (2003)

[33] R. Peverati, D.G. Truhlar: Quest for a universal density functional: the accuracy ofdensity functionals across a. broad spectrum of databases in chemistry and physics, Phil. Trans. R. Soc. A **372**, 20120476 (2016)

[34] A. Stroppa, G. Kresse: The shortcomings of semi-local and hybrid functionals: what we can learn from surface science studies, New Journal of Physics **10**, 063020 (2008)

[35] A.M. Reilly, Tkachenko: van der Waals dispersion interactions in molecular materials: beyond pairwise additivity, Chem. Sc. **6**, 3289 (2015)

[36] J. Klimes, A. Michaelides: Perspective: Advances and challenges in treating van der Waals dispersion forces in density functional theory, J. Chem. Phys. **137**, 128901 (2012)

[37] C. Berland, V.R. Cooper, K. Lee, E. Schröder, T. Thonhauser, P. Hyldgaard, B.I. Lundqvist: van der Waals forces in density functional theory: a review of the vdW-DF method, Rep. Prog. Phys. **78**, 066501 (2015)

[38] Y. Andersson, D.C. Langreth, B.I. Lundqvist: van der Waals Interactions in Density-Functional Theory, Phys. Rev. Lett. **76**, 102 (1996)

[39] D.C. Langreth, M. Dion, H. Ryberg, E. Schröder, P. Hyldgaard, B.I. Lundqvist: Van der Waals Density Functional Theory with Applications, International Journal of Quantum Chemistry **101**, 599 (2005)

[40] M. Dion, H. Ryberg, E. Schröder D.C. Langreth, B.I. Lundqvist: Van der Waals Density Functional for General Geometries, Phys. Rev. Lett. **92**, 246401 (2005)

[41] K. Lee, E.D. Murray, L. Kong, B.I. Lundqvist, D.C. Langreth: Higher-accuracy van der Waals density functional, Phys. Rev. B **82**, 081101(R) (2010)

[42] S.D. Chakarova Käck, E. Schröder, B.I. Lundqvist, D.C. Langreth: Application of van derWaals Density Functional to an Extended System: Adsorption of Benzene and Naphthalene on Graphite, Phys. Rev. Lett **96**, 146107 (2006)

[43] S. Grimme: Semiempirical GGA-Type Density Functional Constructed with a Long-Range Dispersion Correction, J. Comput. Chem. **27**, 1787 (2006)

[44] S. Grimme, J. Antony, S. Ehrlich, H. Krie: A consistent and accurate ab initio dispersion correction DFT-D for the 94 elements H-Pu, J. Chem. Phys. **132**, 154104 (2010)

[45] B. Shanigaram, R.K. Chitumalla, K.Bhanuprakash: Adsorption of TCNQ and F4-TCNQ molecules on hydrogen-terminated Si(111) surface: van der Waals interactions included DFT study of the molecular orientations, Computational and Theoretical Chemistry **1084**, 174 (2016)

[46] A. Tkatchenko, M. Scheffler: Accurate Molecular Van Der Waals Interactions from Ground-State Electron Density and Free-Atom Reference Data, Phys. Rev. Lett. **102**, 073005 (2009)

[47] V.G. Ruiz, W. Liu, E. Zojer, M. Scheffler, A. Tkatchenko: Density-Functional Theory with Screened van derWaals Interactions for the Modeling of Hybrid Inorganic-Organic Systems, Phys. Rev. Lett. **108**, 146103 (2012)

[48] E. Zaremba, W. Kohn: Van der Waals interaction between an atom and a solid surface, Phys. Rev. B **13**, 2270 (1976)

[49] W. Liu, V.G. Ruiz, G. Zhang, B. Santra1, X. Ren, M. Scheffler, A. Tkatchenko: Structure and energetics of benzene adsorbed on transition-metal surfaces: density-functional theory with van der Waals interactions including collective substrate response, New Journal of Physics 15 **15**, 053046 (2013)

[50] W. Liu, A. Tkatchenko, M. Scheffler: Modeling Adsorption and Reactions of Organic Molecules at Metal Surfaces, Acc. Chem. Res. **108**, 47 (2014)

[51] L. Schimka, J. Harl, A. Stroppa, A. Gruneis, M. Marsman, F. Mitterdorfer, G. Kresse: Accurate surface and adsorption enegies from may-body pertubation theory, Nature Materials **9**, 741 (2010)

[52] Filippo De Angelis, Antonio Tilocca, Annabella Selloni: Time-Dependent DFT Study of $[Fe(CN)_6]^{4-}$ Sensitization of TiO_2 Nanoparticles, J. Am. Chem. Soc. **126**, 15024 – 15025 (2004)

[53] Thomas Stecher, Karsten Reuter, Harald Oberhofer: First-Principles Free-Energy Barriers for Photoelectrochemical Surface Reactions: Proton Abstraction at TiO_2(110), Phys. Rev. Lett. **117**, 276001 (2016)

[54] A.A. Herzing, C.J. Kiely, A.F. Carley, P. Landon, G.J. Hutchings, H.-J. Freund: Identification of active gold nanoclusters on iron oxide supports for CO oxidation, Science **321**, 1331 (2008)

[55] H.-J. Freund: Models for heterogeneous catalysts: studies at the atomic level, Rend. Fis. Acc. Lincei, doi:10.1007/s12210-016-0560-4 (2016)

[56] M. Schlüter, J.R. Chelikowsky, S.G. Louie, M.L. Cohen: Self-consistent pseudopotential calculations for Si (111) surfaces: Unreconstructed (11) and reconstructed (21) model structures, Phys. Rev. B **15**, 4200 (1975)

[57] M.P. Teter M. Payne, D.C. Allan, T.A. Arias, J.D. Joannopoulos: Iterative minimization techniques for ab initio total- energy calculations: molecular dynamics and conjugate gradients, Rev. Mod. Phys. **64**, 1045 (1992)

[58] R.M. Martin: *Electronic Structure: Basic Theory and Practical Methods* (Cambridge University Press, Cambridge, UK 2004)

[59] T.B. Grimley, C. Pisani: Chemisorption theory in the Hartree-Fock approximation, J. Phys. C: Solid State Phys. **7**, 2831 (1974)

[60] A.R. Williams, P.J. Feibelman, N.D. Lang: Green's-function methods for electronic-structure calculations, Phys. Rev. B **26**, 5433 (1982)

[61] J. Bormet, J. Neugebauer, M. Scheffler: Chemical trends and bonding mechanisms for isolated adsorbates on Al(111), Phys. Rev. B **49**, 17242 (1994)

[62] C. Pisani, F. Corá, R. Nada, R. Orlando: Hartree-Fock perturbed-cluster treatment of local defects in crystals I. The EMBED program: general features, Computer Physics Communications **82**, 139 (1994)

[63] S. Krüger, N. Rosch: The moderately-large-embedded-cluster method for metal surfaces; a density-functional study of atomic adsorption, J. Phys.: Condens. Matter **6**, 8149 (1994)

[64] N. Govind, Y.A. Wang, E.A. Carter: Electronic-structure calculations by first-principles density-based embedding of explicitly correlated systems, J. Chem. Phys. **110**, 7677 (1999)

[65] J.E. Inglesfield: A method of embedding, J. Phys. C: Solid State Phys. **14**, 3795 (1981)

[66] M.I. Trioni, G.P. Brivio, S. Crampin, J.E. Inglesfield: Embedding approach to the isolated adsorbate, Phys. Rev. B **53**, 8052 (1996)

[67] H. Ishida: Surface-embedded Green-function method: A formulation using a linearized-augmented-plane-wave basis set, Phys. Rev. B **63**, 165409 (2001)

[68] J.E. Inglesfield: *The Embedding Method for Electronic Structure*, 1 edn. (Institute of Physics Publishing, Bristol, UK 2016)

[69] G.P. Brivio, G. Butti, S. Caravati, G. Fratesi, M.I. Trioni: Theoretical approaches in adsorption: alkali adatom investigations, J. Phys.: Condens. Matter **19**, 305005 (2007)

[70] M. Brandbyge, J.-L. Mozos, P. Ordejon, J. Taylor, K. Stokbro: Density-functional method for nonequilibrium electron transport, **65**, 165401 (2002)

[71] G. Fratesi, C. Motta, M.I. Trioni, G.P. Brivio, Daniel Sánchez-Portal: Resonant Lifetime of Core-Excited Organic Adsorbates from FirstPrinciples, J. Phys. Chem. C **118**, 8775 (2014)

[72] D. Cvetko, G. Fratesi, G. Kladnik, A. Cossaro, G.P. Brivio, L. Venkataraman, A. Morgante: Ultrafast electron injection into photo-excited organic molecules, Phys. Chem. Chem. Phys. **18**, 8264 (2016)

[73] P. Persson, M.J. Lundqvist, R. Ernstorfer, W.A. Goddard III, F. Willig: Quantum Chemical Calculations of the Influence of Anchor-Cum-Spacer Groups on Femtosecond Electron Transfer Times in Dye-Sensitized Semiconductor Nanocrystals, J. Chem. Theory Comput. **2**, 441 (2006)

[74] W. Shockley: On the Surface States Associated with a Periodic Potential, Phys. Rev **56**, 317 (1939)

[75] I. Tamm: On the possible bound states of electrons on a crystal surfacen the Surface States Associated with a Periodic Potential, Phys. Z. Soviet Union **1**, 733 (1932)

[76] M.C. Desjonqueres, D. Spanjaard: *Concepts in Surface Physics*, 2 edn. (Springer Verlag, Berlin, Heidelberg, Germany 2013)

[77] H. Lüth: *Solid Surfaces, Interfaces and Thin Films*, 5 edn. (Springer Verlag, Berlin, Heidelberg, Germany 2010)

[78] T.B. Grimley: The Molecular Orbital Theory of the Interaction between an Atom and a Crystal Surface, Proc. Phys. Soc. **72**, 103 (1958)

[79] P.O. Gartland, B.J. Slagsvold: Transitions conserving parallel momentum in photoemission from the (111) face of copper, Phys. Rev. B **12**, 4047 (1975)

[80] S.D. Kevan: Evidence for a New Broadening Mechanism in Angle-Resolved Photoemission from Cu(111), Phys. Rev. Lett. **50**, 526 (1983)

[81] S. Caravati, G. Butti, G.P. Brivio, M.I. Trioni, S. Pagliara, G. Ferrini, G. Galimberti, E. Pedersoli, C. Giannetti, F. Parmigiani: Cu(111) and Cu(001) surface electronic states. Comparison between theory and experiment, Surf. Sci. **600**, 3901 (2006)

[82] A. Zangwill: *Physics at Surfaces* (Cambridge University Press, Cambridge, UK 1988)

[83] M. Milun, P. Pervan, D P Woodruff: Quantum well structures in thin metal films: simple model physics in reality?, Rep. Prog. Phys. **65**, 99 (2002)

[84] N.D. Lang, W. Kohn: Theory of Metal Surfaces: Induced Surface Charge and Image Potential, Phys. Rev. B **7**, 3541 (1972)

[85] E.V. Chulkov, V.M. Silkin, P.M. Echenique: Image potential states on metal surfaces: binding energies and wave functions, Surf. Sci. **437**, 330 (1999)

[86] A. Manchon, H.C. Koo, J. Nitta, S.M. Frolov, R.A. Duine: New perspectives for Rashba spinorbit coupling, Nature Materials **14**, 871 (2015)

[87] T. Nakazawa, N. Takagi, M. Kawai, H. Ishida, R. Arafune: Rashba splitting in an image potential state investigated by circular dichroism two-photon photoemission spectroscopy, Phys. Rev. B **94**, 115412 (2016)

[88] P.M. Echeniquea, R. Berndt, E.V. Chulkova, Th. Fauster, A. Goldmanne, U. Hoand E.V. Chulkov, V.M. Silkin, P.M. Echenique: Decay of electronic excitations at metal surfaces, Surf. Sci. Rep. **52**, 213 (2004)

[89] G. Onida, L. Reining, A. Rubio: Electronic excitations: density-functional versus many-body Greens-function approaches, Rev. Mod. Phys. **74**, 601 (2002)

[90] J. Kliewer, R. Berndt, E.V. Chulkov, V.M. Silkin, P.M. Echenique, S. Crampin: Decay of electronic excitations at metal surfaces, Science **288**, 1399 (2000)

[91] S.Å. Lindgren, L. Walldén: Cu surface state and Cs valence electrons in photoelectron spectra from the Cu(111)/Cs adsorption system, Sol. St. Commun. **28**, 283 (1978)

[92] D.A. Eastman F.J. Himpsel, J.A. Knapp: Angle resolved photoemission study of the electronic structure of chemisorbed hydrogen on Ni(111), Phys. Rev. B **19**, 2872 (1979)

[93] S.Å. Lindgren, J. Pauland L. Walldén: Surface state energy shifts by molecular adsorption: Co on clean and Na covered Cu(111), Surf. Sci. **117**, 426 (1982)

[94] S.-Y. Hong, P.-O. Yeh, I. Lee, J. Yu, J.I. Dadap, C. Nuckolls, R.M. Osgood: Coverage-Dependent Modification of the Surface Electronic Structure of an Organic-Semiconductor-Adsorbate Layer, J. Phys. Chem. C **118**, 6214 (2014)

[95] A. Bendounan, S. Ait-Ouazzou: Role of the Shockley State in Doping of Organic Molecule Monolayer, J. Phys. Chem. C **120**, 11456 (2016)

[96] P.A. Sloan, S. Sakulsermsuk, R.E. Palmer: Nonlocal Desorption of Chlorobenzene Molecules from the Si(111)(7×7)Surface by Charge Injection from the Tip of a Scanning Tunneling Microscope: Remote Control of Atomic Manipulation, Phys. Rev. Lett. **105**, 048301 (2010)

[97] A. Manchon, H. C. Koo, J. Nitta, S. M. Frolov, R. A. Duine: New perspectives for Rashba spin-orbit coupling, Nat. Mater. **14**, 871 – 882 (2015)

[98] T.B. Grimley: The molecular orbital theory of interaction between an atom and a crystal surface, Proc. Phys. Soc. Sect A **72**, 103 (1958)

[99] T.B. Grimley: The indirect interaction between atoms or molecules adsorbed on metals, Proc. Phys. Soc. Sect A **90**, 751 (1967)

[100] D.M. Newns: Self-consistent model of hydrogen chemisorption, Phys. Rev. **178**, 1123 (1969)

[101] B. Hammer, J.K. Norskov: Theoretical surfarce science and catalysis-calculations and concepts, Advances in Catalysis **45**, 71 (2000)

[102] Irving Langmuir: Vapor pressures, evaporation, condensation and adsorption, J. Am. Chem. Soc. **54**, 2798 (1932)

[103] R. W. Gurney: Theory of Electrical Double Layers in Adsorbed Films, Phys. Rev. **47**, 479 (1935)

[104] J. Bormet, J. Neugebauer, M. Scheffler: Chemical trends and bonding mechanisms for isloated adsorbates on Al(111), Phys. Rev. B **49**, 17242 – 17252 (1994)

[105] R. D. Diehl, R. McGrath: Current progress in understanding alkali metal adsorption on metal surfaces, J. Phys.: Condens. Matter **9**, 951 – 968 (1997)

[106] M.I. Trioni, S. Achilli, E.V. Chulkov: Key ingredients of the alkali atom - metal surface interaction: Chemical bonding versus spectral properties, Prog. Surf. Sci. **88**, 160 – 170 (2013)

[107] A. Cucchetti, S. C. Ying: Diffusion of Na atoms on a Cu(001) surface, Phys. Rev. B **60**, 11110 (1999)

[108] G. Alexandrowicz, A. Jardine, H. Hedgeland, W. Allison, J. Ellis: Onset of 3D Collective Surface Diffusion in the Presence of Lateral Interactions: Na/Cu(001), Phys. Rev. Lett. **97**, 145103 (2006)

[109] Guido Fratesi, Gil Alexandrowicz, Mario Trioni, Gian Brivio, William Allison: Crucial electronic contributions to measures of surface diffusion by He atom scattering, Phys. Rev. B **77**, 235444 (2008)

[110] O. Godsi, G. Corem, T. Kravchuk, C. Bertram, K. Morgenstern, H. Hedgeland, A. P. Jardine, W. Allison, J. Ellis, G. Alexandrowicz: How Atomic Steps Modify Diffusion and Inter-adsorbate Forces: Empirical Evidence from Hopping Dynamics in Na/Cu(115), J. Phys. Chem. Lett. **6**, 4165 – 4170 (2015)

[111] M. Cavallini, G. Gallinari, L. Menegretti, G. Scoles, U. Valbusa: Rainbow scattering and the intermolecular potential of argon, Chem. Phys. Lett. **7**, 302 (1970)

[112] G. Boato, P. Cantini, U. Garibaldi, A.C. Levi, R. Spedacini, G.E. Tommei: Diffraction and rainbow in atom surface scattering, J. Phys. C: Solid State **6**, L394 (1973)

[113] G. Brusdeylins, R. B. Doak, J. P. Toennies: Measurement of the dispersion relation for Rayleigh surface phonons of Li(100) by inelastic scattering of surface atoms, Phys. Rev. Lett. **46**, 437 (1981)

[114] G. Fratesi, G. Alexandrowicz, M.I. Trioni, G.P. Brivio, W. Allison: Crucial electronic contributions to measures of surface diffusion by He atom scattering measurement, Phys. Rev. B **77**, 235444 (2008)

[115] J.L.F. Da Silva, C. Stampfl: Trends in adsorption of noble gases He, Ne, Ar, Kr,and Xe on Pd(111)($\sqrt{3} \times 3R30^0$) All-electron density functional calculations, Phys. Rev. B **77**, 045401 (2008)

[116] K.H. Rieder: Surface structural research with atom beams diffraction: Helium versus Neon, Surf. Rev. Lett. **1**, 51 (1994)

[117] M. Petersen, S. Wilke, P. Ruggerone, B. Kohler, M. Scheffler: Scattering of Rare-Gas Atoms at a Metal Surface: Evidence of Anticorrugation of the Helium-Atom Potential Energy Surface and the Surface Electron Density, Phys. Rev. Lett. **76**, 995 (1994)

[118] N. Jean, M.I. Trioni, G.P. Brivio, V. Bortolani: Corrugating and Anticorrugating static interactions in Helium-atom scattering from metals, Phys. Rev. Lett. **92**, 013201 (2004)

[119] A. Picone, M. Riva, G. Fratesi, A. Brambilla, G. Bussetti, M. Finazzi, L. Duò, F. Ciccacci: Enhanced Atom Mobility on the Surface of a Metastable Film, Phys. Rev. Lett. **113**, 046102 (2014)

[120] J. Christopher Love, Lara A. Estroff, Jennah K. Kriebel, Ralph G. Nuzzo, George M. Whitesides: Self-Assembled Monolayers of Thiolates on Metals as a Form of Nanotechnology, Chem. Rev. **105**, 1103 – 1170 (2005)

[121] Willi Auwärter, David cija, Florian Klappenberger, Johannes V. Barth: Porphyrins at interfaces, Nat. Chem. **7**, 105 – 120 (2015)

[122] J. Michael Gottfried: Surface chemistry of porphyrins and phthalocyanines, Surf. Sci. Rep. **70**, 259 – 379 (2015)

[123] Gregor Witte, Christof Wöll: Growth of aromatic molecules on solid substrates for applications in organic electronics, J. Mater. Res. **19**, 1889 – 1916 (2004)

[124] Geetha R Dholakia, M. Meyyappan, Antonio Facchetti, Tobin J. Marks: Monolayer to Multilayer Nanostructural Growth Transition in N-Type Oligothiophenes on Au(111) and Implications for Organic Field-Effect Transistor Performance, Nano Lett. **6**, 2447 – 2455 (2006)

[125] Ching-Hsun Chao, Chien-Hung Chan, Fu-Chiao Wu, Jung-Jie Huang, Shui Yang Lien, Ko-Wei Weng, Horng-Long Cheng: Efficient hybrid organic/inorganic photovoltaic cells utilizing n-type pentacene and intrinsic/p-type hydrogenated amorphous silicon, Sol. Energy Mater. Sol. Cells **95**, 2407 – 2411 (2011)

[126] V. C. Sundar: Elastomeric Transistor Stamps: Reversible Probing of Charge Transport in Organic Crystals, Science **303**, 1644 – 1646 (2004)

[127] Yen-Yi Lin, D.I. Gundlach, S.F. Nelson, T.N. Jackson: Pentacene-based organic thin-film transistors, IEEE Trans. Electron Devices **44**, 1325 – 1331 (1997)

[128] Y.-Y. Lin, D.J. Gundlach, S.F. Nelson, T.N. Jackson: Stacked pentacene layer organic thin-film transistors with improved characteristics, IEEE Electron Device Lett. **18**, 606 – 608 (1997)

[129] Ulrike Diebold: The surface science of titanium dioxide, Surf. Sci. Rep. **48**, 53 – 229 (2003)

[130] Chi Lun Pang, Robert Lindsay, Geoff Thornton: Structure of Clean and Adsorbate-Covered Single-Crystal Rutile TiO_2 Surfaces, Chem. Rev. **113**, 3887 – 3948 (2013)

[131] Guido Fratesi, Valeria Lanzilotto, Stefano Stranges, Michele Alagia, Gian Paolo Brivio, Luca Floreano: High resolution NEXAFS of perylene and PTCDI: a surface science approach to molecular orbital analysis, Phys. Chem. Chem. Phys. **16**, 14834 – 14844 (2014)

[132] Valeria Lanzilotto, Carlos Sanchez-Sanchez, Gregor Bavdek, Dean Cvetko, Maria F. Lopez, Jose A. Martin-Gago, Luca Floreano: Planar Growth of Pentacene on the Dielectric TiO_2 (110) Surface, J. Phys. Chem. C **115**, 4664 – 4672 (2011)

[133] Michele Alagia, Chiara Baldacchini, Maria Grazia Betti, Fabio Bussolotti, Vincenzo Carravetta, Ulf Ekström, Carlo Mariani, Stefano Stranges: Core-shell photoabsorption and photoelectron spectra of gas-phase pentacene: Experiment and theory, J. Chem. Phys. **122**, 124305 (2005)

[134] Guido Fratesi, Valeria Lanzilotto, Luca Floreano, Gian Paolo Brivio: Azimuthal Dichroism in Near-Edge X-ray Absorption Fine Structure Spectra of Planar Molecules, J. Phys. Chem. C **117**, 6632 – 6638 (2013)

[135] Gregor Bavdek, Albano Cossaro, Dean Cvetko, Cristina Africh, Cecilia Blasetti, Friedrich Esch, Alberto Morgante, Luca Floreano: Pentacene Nanorails on Au(110), Langmuir **24**, 767 – 772 (2008)

[136] Anu Baby, Guido Fratesi, Shital R. Vaidya, Laerte L. Patera, Cristina Africh, Luca Floreano, Gian Paolo Brivio: Anchoring and Bending of Pentacene on Aluminum (001), J. Phys. Chem. C **119**, 3624 – 3633 (2015)

[137] T. Suzuki, D.C. Sorescu, J.T. Yates: The chemisorption of pentacene on Si(001)-2×1, Surf. Sci. **600**, 5092 – 5103 (2006)

[138] Han-Koo Lee, Jin-hee Han, Ki-jeong Kim, Tai-Hee Kang, Bongsoo Kim: Configuration of pentacene ($C_{22}H_{14}$) films on Si(100)-2×1 studied by NEXAFS, Surf. Sci. **601**, 1456 – 1460 (2007)

[139] Toshihiro Shimada, Hiroyuki Nogawa, Tetsuya Hasegawa, Ryusuke Okada, Hisashi Ichikawa, Keiji Ueno, Koichiro Saiki: Bulk-like pentacene epitaxial films on hydrogen-terminated Si(111), Appl. Phys. Lett. **87**, 061917 (2005)

[140] Kevin P. Weidkamp, Rudolf M. Tromp, Robert J. Hamers: Epitaxial Growth of Large Pentacene Crystals on Si(001) Surfaces Functionalized with Molecular Monolayers, J. Phys. Chem. C **111**, 16489 – 16497 (2007)

[141] P. G. Schroeder, C. B. France, J. B. Park, B. A. Parkinson: Energy level alignment and two-dimensional structure of pentacene on Au(111) surfaces, J. Appl. Phys. **91**, 3010 (2002)

[142] M. Pedio, B. Doyle, N. Mahne, A. Giglia, F. Borgatti, S. Nannarone, S.K.M. Henze, R. Temirov, F.S. Tautz, L. Casalis, et al.: Growth of pentacene on Ag(111) surface: A NEXAFS study, Appl. Surf. Sci. **254**, 103 – 107 (2007)

[143] Daniel Lüftner, Thomas Ules, Eva Maria Reinisch, Georg Koller, Serguei Soubatch, F. Stefan Tautz, Michael G. Ramsey, Peter Puschnig: Imaging the wave functions of adsorbed molecules, Proc. Natl. Acad. Sci. **111**, 605 – 610 (2014)

[144] Kenji Toyoda, Ikutaro Hamada, Kyuho Lee, Susumu Yanagisawa, Yoshitada Morikawa: Density functional theoretical study of pentacene/noble metal interfaces with van der Waals corrections: Vacuum level shifts and electronic structures, J. Chem. Phys. **132**, 134703 (2010)

[145] Andrea Ferretti, Chiara Baldacchini, Arrigo Calzolari, Rosa Di Felice, Alice Ruini, Elisa Molinari, Maria Betti: Mixing of Electronic States in Pentacene Adsorption on Copper, Phys. Rev. Lett. **99**, 046802 (2007)

[146] Kathrin Müller, Ari P. Seitsonen, Thomas Brugger, James Westover, Thomas Greber, Thomas Jung, Abdelkader Kara: Electronic Structure of an Organic/Metal Interface: Pentacene/Cu(110), J. Phys. Chem. C **116**, 23465 – 23471 (2012)

[147] M Simeoni, S Picozzi, B Delley: An ab-initio study of pentacene on aluminum (100) surface, Surf. Sci. **562**, 43 – 52 (2004)

[148] Elena Molteni, Giancarlo Cappellini, Giovanni Onida, Guido Fratesi: Optical properties of organically functionalized silicon surfaces: Uracil-like nucleobases on Si(001), Phys. Rev. B **95**, 075437 (2017)

[149] Anu Baby, He Lin, Gian Paolo Brivio, Luca Floreano, Guido Fratesi: Core-level spectra and molecular deformation in adsorption: V-shaped pentacene on Al(001), Beilstein J. Nanotechnol. **6**, 2242 – 2251 (2015)

[150] Paul Bagus, Daniel Käfer, Gregor Witte, Christof Wöll: Work Function Changes Induced by Charged Adsorbates: Origin of the Polarity Asymmetry, Phys. Rev. Lett. **100**, 126101 (2008)

[151] Guido Fratesi: Potential energy surface of alkali atoms adsorbed on Cu(001), Phys. Rev. B **80**, 045422 (2009)

[152] C. A. Papageorgopoulos: Studies of separate adsorption and coadsorption of Cs and O_2 on Cu(100), Phys. Rev. B **25**, 3740 – 3749 (1982)

[153] Guido Fratesi, Andrea Pace, Gian Paolo Brivio: Short-range lateral interactions and depolarization of Na atoms on Cu surfaces, J. Phys. Condens. Matter **22**, 304005 (2010)

[154] D. A. MacLaren, C. Huang, A. C. Levi, W. Allison: Coverage-dependent quantum versus classical scattering of thermal neon atoms from Li/Cu(100), J. Chem. Phys. **129**, 094706 (2008)

[155] Guido Fratesi: Depolarization and bonding in quasi-one-dimensional Na structures on Cu(001), Phys. Rev. B **84**, 155424 (2011)

[156] Andrew P. Graham, J. Peter Toennies: Helium-atom diffraction study of the submonolayer structures of sodium on Cu(001), Phys. Rev. B **56**, 15378 – 15390 (1997)

[157] Congcong Huang, G. Fratesi, D. A. MacLaren, Weidong Luo, G. P. Brivio, W. Allison: Charge redistribution in the formation of one-dimensional lithium wires on Cu(001), Phys. Rev. B **82**, 081413 (2010)

[158] P.K. Johnny Wong, Wen Zhang, Gerrit van der Laan, Michel P. de Jong: Hybridization-induced charge rebalancing at the weakly interactive C60/Fe3O4(001) spinterface, Org. Electron. **29**, 39 – 43 (2016)

[159] Yu-Hsun Chu, Chuang-Han Hsu, Chun-I Lu, Hung-Hsiang Yang, Tsung-Han Yang, Chi-Hung Luo, Kai-Jheng Yang, Shih-Hao Hsu, Germar Hoffmann, Chao-Cheng Kaun, et al.: Spin-Dependent Molecule Symmetry at a Pentacene-Co Spinterface, ACS Nano **9**, 7027 – 7032 (2015)

[160] H. Wende, M. Bernien, J. Luo, C. Sorg, N. Ponpandian, J. Kurde, J. Miguel, M. Piantek, X. Xu, Ph. Eckhold, et al.: Substrate-induced magnetic ordering and switching of iron porphyrin molecules, Nat. Mater. **6**, 516 – 520 (2007)

[161] Simone Casolo, Ole Martin Lovvik, Rocco Martinazzo, Gian Franco Tantardini: Understanding adsorption of hydrogen atoms on graphene, J. Chem. Phys. **130**, 054704 (2009)

[162] Elton J G Santos, Andrés Ayuela, Daniel Sánchez-Portal: Universal magnetic properties of sp_3-type defects in covalently functionalized graphene, New J. Phys. **14**, 043022 (2012)

[163] He Lin, Guido Fratesi, Gian Paolo Brivio: Graphene magnetism induced by covalent adsorption of aromatic radicals, Phys Chem Chem Phys **17**, 2210 – 2215 (2014)

[164] Elton J. G. Santos, D. Sánchez-Portal, A. Ayuela: Magnetism of covalently functionalized carbon nanotubes, Appl. Phys. Lett. **99**, 062503 (2011)

[165] Rocco Martinazzo: *Graphene science handbook. Nanostructure and atomic arrangement*, ed. by Mahmood Aliofkhazraei, Nasar Ali, W. I. Milne, Cengiz S. Ozkan, Stanislaw Mitura, Juana L. Gervasoni (CRC Press, Taylor & Francis Group, Boca Raton 2016)

[166] Jannik C. Meyer, C. O. Girit, M. F. Crommie, A. Zettl: Imaging and dynamics of light atoms and molecules on graphene, Nature **454**, 319 – 322 (2008)

[167] Richard Balog, Bjarke Jørgensen, Louis Nilsson, Mie Andersen, Emile Rienks, Marco Bianchi, Mattia Fanetti, Erik Lægsgaard, Alessandro Baraldi, Silvano Lizzit, et al.: Bandgap opening in graphene induced by patterned hydrogen adsorption, Nat. Mater. **9**, 315 – 319 (2010)

[168] Jayakumar Balakrishnan, Gavin Kok Wai Koon, Manu Jaiswal, A. H. Castro Neto, Barbaros Özyilmaz: Colossal enhancement of spin-orbit coupling in weakly hydrogenated graphene, Nat. Phys. **9**, 284 – 287 (2013)

[169] A.A. Komlev, T.L. Makarova, E. Lahderanta, P.V. Semenikhin, A.I. Veinger, T.V. Tisnek, G. Magnani, G. Bertoni, D. Pontiroli, M. Ricco: Magnetism of aniline modified graphene-based materials, J. Magn. Magn. Mater. **415**, 45 – 50 (2016)

[170] J. Ben Taylor, Louise C. Mayor, Janine C. Swarbrick, James N. OShea, Cristina Isvoranu, Joachim Schnadt: Adsorption and charge transfer dynamics of biisonicotinic acid on Au(111), J. Chem. Phys. **127**, 134707 (2007)

[171] Abhilash Ravikumar, Anu Baby, He Lin, Gian Paolo Brivio, Guido Fratesi: Femtomagnetism in graphene induced by core level excitation of organic adsorbates, Sci. Rep. **6**, 24603 (2016)

List of abbreviations

(DFT) density functional theory
(KS) Kohn-Sham
(LDA) local density approximation
(SLDA) local spin density approximation
(GGA) generalized gradient approximation
(PW91) Perdew, Wang 1991
(PBE) Perdew, Burke, Ernzerhof
(SIC) self-interaction correction
(HF) Hartree-Fock
(B3LYP) Becke, Lee, Yang, and Parr
(vdW) van der Waals
(PTCDA) perylene-3,4,9,10-tetracarboxylic dianhydride
(TDDFT) Time Dependent Density Functional Theory
(ARPES) angle resolve photoemission spectroscopy
(QW) quantum well
(IP) image potential
(IPS) image potential state
(2PP) two photon photoemission
(IPES) inverse photoemission spectroscopy
(STS) scanning tunneling spectroscopy
(RPA) random phase approximation
(HBC) hexa-catahexabenzocoronene
(NTCDA) 1,4,5,8-naphtalene tetracarboxylic dianhydride
(fcc) face centered cubic site
(hcp) hexagonal close packed
(HAS) Helium atom scattering
(LEED) low energy electron diffraction
(SAM) self-assembled monolayers
(PAH) policyclic aromatic hydrocarbons
(NEXAFS) near edge X-ray absorption fine structure
(LUMO) lowest unoccupied molecular orbital
(HOMO) highest occupied molecular orbital
(RHEED) reflection high-energy electron diffraction

Contents